AFWAL-TR-80-3010

ADA084172

FLUTTER ANALYSIS OF A TWO-DIMENSIONAL AND TWO-DEGREE-OF-FREEDOM SUPERCRITICAL AIRFOIL IN SMALL-DISTURBANCE UNSTEADY TRANSONIC FLOW

T. Y. YANG
P. GURUSWAMY
A. G. STRIZ

PURDUE UNIVERSITY
WEST LAFAYETTE, INDIANA 47907

DTIC
S ELECTE D
MAY 1 5 1980
B

MARCH 1980

TECHNICAL REPORT AFWAL-TR-80-3010
Final Report for period November 1978 — November 1979

Approved for public release; distribution unlimited.

DDC FILE COPY

FLIGHT DYNAMICS LABORATORY
AIR FORCE WRIGHT AERONAUTICAL LABORATORIES
AIR FORCE SYSTEMS COMMAND
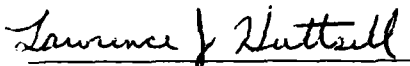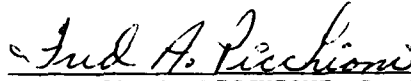WRIGHT-PATTERSON AIR FORCE BASE, OHIO 45433

80 5 9 018

NOTICE

When Government drawings, specifications, or other data are used for any purpose other than in connection with a definitely related Government procurement operation, the United States Government thereby incurs no responsibility nor any obligation whatsoever; and the fact that the government may have formulated, furnished, or in any way supplied the said drawings, specifications, or other data, is not to be regarded by implication or otherwise as in any manner licensing the holder or any other person or corporation, or conveying any rights or permission to manufacture, use, or sell any patented invention that may in any way be related thereto.

This report has been reviewed by the Information Office (OI) and is releasable to the general public, including foreign nations.

This technical report has been reviewed and is approved for publication.

LAWRENCE J. HUTTSELL
Aerospace Engineer
Aeroelastic Group

FREDERICK A. PICCHIONI, Lt Col, USAF
Ch, Analysis and Optimization Branch

FOR THE COMMANDER

RALPH L. KUSTER, Jr, Col, USAF
Chief, Structures and Dynamics Division

Copies of this report should not be returned unless return is required by security considerations, contractual obligations, or notice on a specific document.

REPORT DOCUMENTATION PAGE	READ INSTRUCTIONS BEFORE COMPLETING FORM

1. REPORT NUMBER	2. GOVT ACCESSION NO.	3. RECIPIENT'S CATALOG NUMBER
AFWAL-TR-80-3010	AD-A084 172	

4. TITLE (and Subtitle)	5. TYPE OF REPORT & PERIOD COVERED
Flutter Analysis of a Two-Dimensional and Two-Degree-of-Freedom Supercritical Airfoil in Small-Disturbance Unsteady Transonic Flow	Final Report. November 1978-October 1979
	6. PERFORMING ORG. REPORT NUMBER

7. AUTHOR(s)	8. CONTRACT OR GRANT NUMBER(s)
T.Y. Yang, P. Guruswamy, and Alfred G. Striz	AFOSR-78-3523A

9. PERFORMING ORGANIZATION NAME AND ADDRESS	10. PROGRAM ELEMENT, PROJECT, TASK AREA & WORK UNIT NUMBERS
School of Aeronautics and Astronautics Purdue University West Lafayette, IN 47907	PE 61102F 2307/N5/11

11. CONTROLLING OFFICE NAME AND ADDRESS	12. REPORT DATE
Air Force Wright Aeronautical Laboratories (FIBR) Wright-Patterson AFB, OH 45433	March 1980
	13. NUMBER OF PAGES 90

14. MONITORING AGENCY NAME & ADDRESS(if different from Controlling Office)	15. SECURITY CLASS. (of this report)
	15a. DECLASSIFICATION/DOWNGRADING SCHEDULE

16. DISTRIBUTION STATEMENT (of this Report)

Approved for public release, distribution unlimited.

17. DISTRIBUTION STATEMENT (of the abstract entered in Block 20, if different from Report)

18. SUPPLEMENTARY NOTES

19. KEY WORDS (Continue on reverse side if necessary and identify by block number)

Airfoils
Flutter
Supercritical
Transonic
Unsteady Aerodynamics

20. ABSTRACT (Continue on reverse side if necessary and identify by block number)

Flutter analysis is performed for a MBB A-3 supercritical airfoil at transonic Mach numbers. Two degrees of freedom, pitching and plunging, are considered. The unsteady aerodynamic data are obtained by using two separate transonic aerodynamic computational codes: (1) LTRAN2 based on the time integration method and (2) STRANS2 and UTRANS2 based on the harmonic analysis method.

(cont.)

DD FORM 1473
1 JAN 73

The steady aerodynamic results are shown in the form of upper and lower surface pressure curves. The unsteady aerodynamic coefficients are obtained and tabulated for various values of low reduced frequency by pitching the MBB A-3 airfoil about the quarter chord axis. For the case of zero mean angle of attack, the coefficients obtained by the two computer codes are directly compared and discussed.

At design Mach number of 0.765 and zero mean angle of attack, flutter results are obtained by both methods and compared. They are presented as plots of flutter speed and the corresponding reduced frequency vs. one of the four parameters: airfoil - air mass ratio; position of mass center; position of elastic axis; and plunge-to-pitch frequency ratio.

To study the effects of camber and thickness distribution of the MBB A-3 supercritical airfoil at the design conditions, flutter results are obtained for three different models of airfoil: (1) the supercritical MBB A-3 airfoil; (2) a MBB A-3 airfoil without camber; and (3) a NACA 64A010 airfoil scaled down to a maximum thickness-to-chord ratio of 8.9%, same as that of the supercritical MBB A-3 airfoil. The design Mach number used is 0.765 and the angles of attack are chosen to be 0.42° for LTRAN2 and 0.75° for STRANS2 so that both programs yield the same value of design steady lift coefficient, $C_{\ell} = 0.58$. Results are presented as plots of flutter speed and the corresponding reduced frequency vs. one of the four aeroelastic parameters as mentioned in last paragraph. For most of the aeroelastic parameters studied, it is found that removal of the camber from model 1 reduces the flutter speed. It is also found that the flutter characteristics of models 2 and 3 are almost the same. The supercritical thickness distribution does not appear to have a different effect on aerodynamic coefficients and flutter speed from the conventional thickness distribution.

The effect of Mach number on flutter speed is studied for the MBB A-3 supercritical airfoil at zero mean angle of attack. The Mach numbers considered are M = 0.70, 0.72, 0.74, 0.765, and 0.78, respectively. Two sets of curves for flutter speed are plotted against Mach numbers while one of the four aeroelastic parameters is varied. The two sets of curves, based on two separate computational methods, are in good agreement in trend and in fairly good agreement in magnitude. The transonic dip phenomenon is observed in all curves. The effect of eac aeroelastic parameter on the curves is studied.

FOREWORD

This report was prepared by Professor T.Y. Yang of the School of
Aeronautics and Astronautics of Purdue University under AFOSR Grant 78-3523A,
"Application of Time-Accurate Transonic Aerodynamics to Aeroelastic Problems".
The research was administered by Lawrence J. Huttsell of the Structures and
Dynamics Division, Flight Dynamics Laboratory, Wright-Patterson Air Force
Base, Ohio.

The report covers work conducted from November 1978 to October 1979.
T.Y. Yang was the principal investigator. P. Guruswamy and Alfred G. Striz
were the graduate research assistants. Dr. Samuel R. Bland of NASA-Langley
Research Center and Dr. William F. Ballhaus of NASA-Ames Research Center
have been helpful as technical consultants, especially at the early stage
of this project.

DTIC
SELECTED
MAY 1 5 1980
B

ACCESSION for
NTIS   White Section
DDC   Buff Section
UNANNOUNCED
JUSTIFICATION

BY
DISTRIBUTION/AVAILABILITY CODES
Dist.   AVAIL. and/or SPECIAL

A

iii

TABLE OF CONTENTS

TABLE OF CONTENTS   (Continued)

LIST OF ILLUSTRATIONS

LIST OF ILLUSTRATIONS (Continued)

LIST OF TABLES

NOMENCLATURE

a_h	-	distance between mid-chord and elastic axis in semi-chords, positive toward the trailing edge
$[A]$	-	aerodynamic matrix
b	-	semi-chord of the airfoil
c	-	full chord of the airfoil
C_ℓ	-	steady lift coefficient
C_m	-	steady moment coefficient
C_{ℓ_δ}	-	lift coefficient due to plunging
C_{ℓ_α}	-	lift coefficient due to pitching
C_{m_δ}	-	moment coefficient due to plunging
C_{m_α}	-	moment coefficient due to pitching
g	-	structural damping coefficient
g_h	-	damping coefficient for plunging mode
g_α	-	damping coefficient for pitching mode
h	-	plunging degree of freedom, positive downward
I_α	-	polar moment of inertia about elastic axis
k_b	-	$\omega b/U$, reduced frequency with respect to semi-chord length b
k_c	-	$\omega c/U$, reduced frequency with respect to full chord length c
k_h	-	bending stiffness coefficient corresponding to plunging displacement
k_α	-	torsional stiffness coefficient corresponding to pitching rotation
$[K]$	-	matrix of stiffness coefficients
m	-	mass of airfoil per unit span
M or M_∞	-	free stream Mach number
$[M]$	-	mass matrix
Q_h	-	total aerodynamic lifting force
Q_α	-	total aerodynamic moment about pitching axis

r_α - $(I_\alpha/mb^2)^{1/2}$, radius of gyration about elastic axis

s - $(a_h - x_p)/2$

S -   airfoil static moment about elastic axis

U -   free stream velocity

x_p -   distance between mid-chord and pitching axis in semi-chords, positive toward the trailing edge

x_α -   S/mb, distance between elastic axis and center of mass in semi-chords, positive toward the trailing edge

α -   pitching degree of freedom, positive in nose-up direction

α_i -   induced angle of attack

γ -   ratio of specific heats

δ -   h/c

ε -   unsteady perturbation parameter

λ -   flutter eigenvalue

μ - $m/\pi\rho b^2$, airfoil-air mass ratio

ξ -   h/b

ρ -   free stream air density

τ -   ratio of airfoil thickness to chord length

ϕ -   disturbance velocity potential

ω -   flutter frequency of harmonic oscillation

ω_h - $(k_h/m)^{1/2}$, uncoupled plunging frequency

ω_α - $(k_\alpha/I_\alpha)^{1/2}$, uncoupled pitching frequency

ω_r -   reference frequency set equal to unity

SECTION I

INTRODUCTION

In recent years, there has been an increasing trend that aircraft be operated at a speed in high subsonic or transonic regimes. When an airfoil is operated at a speed in the transonic region, shocks form on the airfoil which result in an increase in the drag forces and a loss in lift force due to boundary layer separation. Consequently, there has been a need for improvement in the design of conventional airfoils to reduce such deficiencies and supercritical airfoils have been developed. These advanced airfoils can delay the drag rise Mach number and give higher lift coefficients.

The scope of this report is to study the flutter characteristics of a supercritical airfoil in the transonic regime. The airfoil chosen is a MBB A-3 airfoil designed by Messerschmitt - Bölkow - Blohm of the Federal Republic of Germany.

1.1 Developments of Supercritical Airfoils

Early literature regarding the development of the concept of supercritical airfoil can be found in References 1 and 2. There has been extensive research, conducted both theoretically and experimentally, in the development of supercritical airfoils.

Among the supercritical airfoils developed, the airfoil of the F-8 aircraft is one that has been studied more extensively. A detailed report of such developments is given in Reference 3. This supercritical wing was obtained by modifying the conventional wing of TF-8A airplane. The new configuration was experimentally developed in the eight-foot Transonic Pressure Tunnel at the

1

NASA-Langley Research Center. It was designed for optimum cruise at a
Mach number of 0.99. With this wing the practicality of the supercritical
wing concept was demonstrated by flight tests. The wing demonstrated a
delayed drag rise Mach number and a high buffet-free lift coefficient.
Reference 3 has also provided the F-8 wing flight pressure, boundary-layer
and wake measurements, and comparisons with wind tunnel data.

A comprehensive account of the studies of supercritical airfoils can be
found in the AGARD Conference Proceedings (No. 35) on "Transonic Aerodynamics"
in 1968. In an introductory paper (Reference 4), Nieuwland and Spee discussed
the existence of transonic shock-free flow. The main purpose of the paper
was to present some facts about the fundamental theorems, the time dependent
stability aspects, and the experimental data for the transonic potential flow.

In Reference 5, Vincent de Paul discussed experimental research on super-
critical wing profiles. A family of symmetrical airfoils was selected. The
main purpose was to study some upper-surface velocity distributions having
a peak near the airfoil leading edge. The studies included both subsonic
and transonic Mach numbers.

In Reference 6, Magnus, Gallaher, and Yoshihara discussed an inviscid
supercritical airfoil theory. A finite difference scheme with a concept of ar-
tificial viscosity to account for shocks was presented for computing the
steady planar flow over a prescribed lifting profile. With this method, shock
waves acquire a steep profile appearing at their correct location with proper
jump conditions fulfilled. Two examples were given. The first example showed
the flow at $M_\infty = 0.85$ over a biconvex airfoil of 8.4% thickness-to-chord ratio
at zero angle of attack. Through this example, the ability of the procedure
to evolve shock waves was demonstrated. In the second example, a blunt-nosed

2

shockless profile at zero angle of attack was considered. Results included a discussion of the stability of the shockless flows.

In Reference 7, Lock and Fulker discussed an experimental procedure for designing supercritical airfoils. In the paper, the authors first briefly discussed results on supercritical airfoils designed at the National Physical Laboratory and Royal Aircraft Establishment of the United Kingdom. Then they described the design of a basic airfoil, together with some modifications to it, which were successful in improving its performance at both high and low speeds. It was shown that the best of these airfoils, with thickness-to-chord ratio of 0.105, has a drag rise Mach number of 0.8 at a lift coefficient of 0.5. The supercritical airfoil has a maximum lift coefficient of 1.2 at low speed. The authors compared their experimental results with the theoretical calculations obtained by the finite difference method of Bauer, Garabedian, and Korn which included a partial allowance for viscous effects. They concluded that the theoretical methods needed further improvement before they could be used with confidence for practical purpose.

A detailed description of the design and analysis of supercritical wing sections is given by Bauer, Garabedian, and Korn in References 8, 9, and 10 with Jameson being another author in Reference 9. In Reference 8, the authors presented a mathematical theory based on the finite difference scheme for the design of supercritical wing sections. They presented a computer program for the analysis and also illustrated the method by examples. Several shockless airfoils were designed and tested in the wind tunnel. Their theoretical results established satisfactory agreement with the experimental results.

In Reference 9, the work carried out in Reference 8 was modified and was presented in a more definitive form. The authors improved the design of

the trailing edge by which a lift increase of 15 to 20 percent was obtained.
The improved method has provision to handle supersonic as well as subsonic
free stream Mach numbers, and to capture the shock wave as far back on an
airfoil as required. Moreover, the method led to an effective three-dimensional
program for the computation of transonic flows past an oblique wing. Detailed
comparisons were made with experimental data. The comparisons were favorable.

The work presented in Reference 10 was a sequel to the two earlier
References (8 and 9). New mathematical techniques for the design and analysis
of a supercritical airfoil were incorporated into the computer code. The
advanced mathematical approach made it possible to assign the pressure as a
function of the arc length and then obtain a shockless airfoil that nearly
achieves the desired distribution of pressure. This tool enabled them to
design families of transonic airfoils more easily both for airplane wings
and for compressor blades in cascades.

The iterative process employed in Reference 10 can be summarized as
follows: (1) The airfoil is prescribed and mapped onto the unit circle. The
free stream Mach number is specified and either the coefficient of lift or the
angle of attack can be prescribed; (2) The flow calculations are executed
for a fixed number of cycles; (3) A boundary layer correction is computed and
added to the original airfoil to give a new profile; and (4) The profile is
mapped onto the unit circle. Steps 2 through 4 are repeated till a satisfactory
profile is obtained. The authors illustrated the method with examples.
Results compare well with those from experiment.

In a recent paper (Reference 11), Sobieczky, Yu, Fung, and Seebass presented
a new method for designing shock-free transonic configurations. The method is
based on the principle that if the hodograph method works for specified flow

4

and airfoil parameters, it will also work for a shock-free configuration. Using this method, the authors developed a computer program that can design a two-dimensional inviscid flow potential airfoil in a few seconds of CDC 7600 CPU time. They illustrated the method by designing a supercritical airfoil which is based on the conventional airfoil NACA 64A410.

1.2 Developments in Unsteady Transonic Aerodynamics

Due to the fast growth of digital computers, advances in the numerical computational methods of a transonic flow field around oscillating two-dimensional airfoils have been extensive. Many computer programs have been developed based on these methods. A brief survey of these developments can be found in, for example, Reference 12. It was observed in Reference 12 that the computer programs STRANS2 and UTRANS2 developed by Traci, Albano, and Farr (Reference 13) and the LTRAN2 developed by Ballhaus and Goorjian (Reference 14) can be efficiently used to obtain unsteady transonic aerodynamic data.

The computer programs STRANS2 and UTRANS2 use a harmonic analysis method to solve the two-dimensional, moderate-frequency, small-disturbance transonic equations. The unsteady aerodynamic equations are linearized with respect to time. Thus the unsteady solution is treated as a small linear perturbation over a nonlinear steady state solution. The position of the shock is fixed at the steady state position throughout the analysis. In these programs, both steady and unsteady aerodynamic equations are solved by a mixed differencing line relaxation procedure.

On the other hand, the computer program LTRAN2 is based on the time integration method. This program solves the two-dimensional, low-frequency, small-disturbance transonic equation. The solution for the steady part is obtained by successive line over-relaxation method (SLOR). The solution for

5

the unsteady part is obtained by an alternating-direction implicit finite difference algorithm. In this program the shock is allowed to move during the unsteady analysis.

In the present study, both STRANS2/UTRANS2 and LTRAN2 computer programs were used to obtain the required aerodynamic data.

1.3 Developments in Transonic Aeroelasticity of Conventional Airfoils

Following the recent advances in computational aerodynamics of transonic flows, the research in aeroelastic applications has begun. A detailed account of such research can be found in, for example, References 12 and 15. A comprehensive state-of-the-art review of the developments in transonic aeroelasticity is given by Ashley in Reference 16.

In Reference 12, flutter analysis of two-dimensional and two-degree-of-freedom airfoils in small-disturbance unsteady transonic flow was carried out. Flutter results were obtained for flat plates, a NACA 64A006 airfoil, and a NACA 64A010 airfoil by simultaneously using two transonic aerodynamic computational codes: (1) STRANS2 and UTRANS2 based on harmonic analysis, and (2) LTRAN2 based on the time integration method. The results were presented as plots of flutter speed and the corresponding reduced frequency versus one of the four parameters: airfoil-air mass ratio; position of mass center; position of elastic axis; and free stream Mach number. On each plot, several sets of curves for different values of plunge-to-pitch frequency ratio are shown simultaneously. The contents of the report illustrate the application of transonic computer codes to flutter analysis.

In Reference 15, an aeroelastic response analysis of two-dimensional single- and two-degree-of-freedom airfoils in low frequency, small-disturbance unsteady transonic flow was carried out. The computer code LTRAN2 was employed

6

to obtain the aerodynamic forces. Aeroelastic responses were obtained for
flat plates (single- and two-degree-of-freedom) at $M_\infty = 0.7$ by the linear
part of LTRAN2. The NACA 64A006 airfoil at Mach numbers of 0.88 and 0.85 was
also analyzed. The response results obtained for two-degree-of-freedom systems
for neutrally stable conditions were correlated with those obtained by the
U-g method. Results also included stable and unstable response curves and
their variation with altitude. The validity of the principle of superposition
of airloads in transonic speeds was evaluated in the example studies.

1.4 Developments in Transonic Aeroelasticity of Supercritical Airfoils

Based on the steady aerodynamic data, the supercritical airfoils have
proven to be more efficient than conventional airfoils in the transonic regime.
However, it is of more practical interest to compare the unsteady aerodynamic
data between the two types of airfoils. In that case, aeroelastic characteristics
of the two types of airfoils can be studied and compared and more useful
conclusions can be drawn. Studies of the aeroelastic characteristics of
supercritical airfoils have begun recently.

The first significant experimental study on aeroelastic characteristics
of a supercritical wing was by Farmer and Hanson (Reference 17). A wind
tunnel study was conducted to investigate flutter characteristics of two
dynamically similar wings: one with a supercritical and the other with a
conventional airfoil. The two wings had the same planform, same maximum
thickness-to-chord ratio, and nearly identical stiffness and mass distributions.
The flutter boundaries of the two wings were measured and compared with those
obtained from a subsonic lifting surface theory. It was found that the theory
and experiment correspond well up to $M_\infty = 0.85$. Analytical results did not
indicate the large transonic dip found experimentally for both wings. It

7

was also found that the experimental flutter boundaries of the two wings were nearly identical up to $M_\infty = 0.9$, after that the supercritical wing experienced a much more pronounced transonic dip.

In Reference 18, McGrew et al. carried out a theoretical aeroelastic analysis on supercritical wings. They developed transonic methods by correcting subsonic oscillatory aerodynamic influence coefficients obtained by the doublet lattice method for use in flutter and aerodynamic response analysis of supercritical wings. The corrections were based on steady transonic measured data. The methods were applied to a TF-8A flutter model and a YC-15II prototype aircraft and the results were compared with test data. It was confirmed that supercritical wings exhibit significantly lower flutter speeds than a conventional wing of equal size and rigidities in the high transonic region. It was also demonstrated that these lower flutter speeds could be accurately predicted if the doublet lattice unsteady aerodynamics were properly weighted by the relevant test data.

In Reference 16, Ashley studied the flutter characteristics of a typical section of the TF-8A supercritical wing taken from the 65.3% semispan station. The required aerodynamic data were taken from the wind tunnel test results available from NASA (Reference 3). The selected airfoil section was assumed to have two degrees of freedom, pitch and plunge. The free stream Mach numbers considered were 0.5, 0.8, 0.89, 0.95, and 0.98, respectively. Results were presented as plots of flutter speed versus airfoil-air mass ratio. The influences of Mach number, section normal force coefficient, shock phase lag, and amplitude of shock displacement on flutter speeds for varying airfoil-air mass ratio were considered in detail. It was shown that the flutter speed decreases with the increase in Mach number, section normal force coefficient, shock phase lag, and amplitude of shock displacement, for airfoil-to-air mass

8

ratio varying between 50 and 200. Results also included curves to exemplify the effect of various aerodynamic approximations. Finally, a flutter curve was presented which simulates testing in a facility like the NASA Transonic Dynamics Tunnel.

1.5 Flutter Analysis of a MBB A-3 Supercritical Airfoil

The purpose of this study was to investigate the flutter characteristics of a MBB A-3 supercritical airfoil. The configuration is one of the AGARD standard airfoils suggested for aeroelastic applications of transonic unsteady aerodynamics (Reference 19).

The steady aerodynamic results were obtained by both STRANS2 and LTRAN2 in the form of pressure plots on upper and lower surfaces. The unsteady results were obtained by UTRANS2 (harmonic method) and LTRAN2 (time integration method) in the form of lift and moment aerodynamic coefficients at various values of reduced frequency.

The study was first conducted by considering a case at design Mach number of 0.765 and zero mean angle of attack. Two parallel sets of results for steady pressure distributions, unsteady aerodynamic coefficients, and flutter speed curves were obtained by simultaneously using the two separate computer programs. The two sets of results are in good agreement. The characteristics and trends of the tables and curves are discussed. The effect of each aeroelastic parameter on flutter speed curves is also discussed in this report.

The design conditions of the MBB A-3 supercritical airfoil are: $M_\infty = 0.765$, angle of attack $\alpha = 1.3^o$; and steady lift coefficient $C_\ell = 0.58$. From the steady pressure computations, it was found that at the design Mach number of 0.765 the angles of attack required to produce the design lift coefficient of 0.58 were 0.75^o and 0.42^o by STRANS2 and LTRAN2, respectively. Hence, flutter

9

analyses were performed separately by using angles of attack of 0.75^O and 0.42^O for the two respective computer programs. Results were obtained and discussed in a fashion similar to that performed in the case of zero mean angle of attack.

In order to study the effect of camber on flutter results, a MBB A-3 airfoil without camber was considered. Flutter analyses were performed for design Mach number of 0.765 and at angles of attack of 0.75^O and 0.42^O for STRANS2/UTRANS2 and LTRAN2, respectively. The results show that the camber has a beneficial effect in increasing the flutter speeds.

It was also of interest to study a conventional airfoil of the same maximum thickness-to-chord ratio (8.9%) as that of the MBB A-3 supercritical airfoil. As suggested by AFFDL, a NACA 64A010 airfoil scaled down to 8.9% maximum thickness-to-chord ratio was selected. Similar flutter analysis as mentioned above was carried out for this airfoil. The aerodynamic and flutter results are compared with those obtained for the MBB A-3 supercritical airfoil, with and without camber.

In order to investigate the effect of Mach number, flutter analysis was also carried out for the MBB A-3 supercritical airfoil at five different Mach numbers: 0.7, 0.72, 0.74, 0.765, and 0.78. The angle of attack was assumed to be zero. Flutter curves are presented as plots of flutter speed and the corresponding reduced frequency versus Mach number for various values of different aeroelastic parameters. The "transonic dip" phenomenon is observed and the comparisons of the curves by the two computer programs are favorable.

10

SECTION II

TRANSONIC FLOW EQUATIONS

Developments of numerical procedures for obtaining practical solutions for the unsteady flow around two-dimensional airfoils have been extensive. A number of solution procedures have led to successful transonic codes. The computer codes based on time integration method and harmonic method are two among them. In this section the aerodynamic equations employed in the two codes are discussed.

2.1 Unsteady Two-Dimensional Flow Equation for Transonic Flow

The simplified basic aerodynamic equations, following the assumptions that the flow is two-dimensional, inviscid, transonic ($M_\infty \approx 1$), and that the velocity disturbances are small compared to the free stream velocity U, can be deduced from the general equation of continuity of gas dynamics as

$$k_c^2 M_\infty^2 \phi_{tt} + 2k_c M_\infty^2 \phi_{xt} = V_c \phi_{xx} + \phi_{yy} \tag{1}$$

where $k_c = \omega c/U$ is the reduced frequency; M_∞ is the free stream Mach number; ϕ is the disturbance velocity potential; $V_c = 1 - M_\infty^2 - (\gamma + 1)M_\infty^m \phi_x$; m is a function of M_∞; and γ is the ratio of specific heats.

In deriving the above equation, the coordinate system is fixed with respect to the airfoil, and x is aligned with the free stream direction. The flow is defined as locally subsonic or supersonic, relative to the fixed coordinate system, for $V_c > 0$ or $V_c < 0$, respectively. A measure of the degree of unsteadiness is given by the reduced frequency k_c when the airfoil is oscillating periodically with a frequency ω.

Several numerical approaches have been developed for the solution of transonic flow fields governed by Equation 1.

2.2 Harmonic Method

In the harmonic method it is assumed that the flow field for some sinusoidal body motion of frequency ω can be expressed in the form

$$\phi(x,y,t) = \phi_0(x,y) + \epsilon\phi_1(x,y)e^{i\omega t} + \epsilon^2\phi_1^2(x,y)e^{i\omega t}$$

$$+ \text{ higher-order terms} \tag{2}$$

where ϕ is the disturbance velocity potential, and ϵ is related to the amplitude of body motion. For purely subsonic or supersonic flows, the sinusoidal motion produces a sinusoidal response ϕ at the same frequency and all higher-order terms are zero. This is not true in the transonic case, in which a higher harmonic content in ϕ results because the governing equations are nonlinear. However, if the amplitudes of motion are assumed to be very small ($\epsilon \ll 1$), terms of order ϵ^2 or higher can still be neglected. Hence, equation 2 can be written as

$$\phi(x,y,t) = \phi_0(x,y) + \epsilon\phi_1(x,y)e^{i\omega t} \tag{3}$$

In Equation 3, the solution for ϕ_1 depends on the mean steady-state solution ϕ_0. In this equation it is implied that the unsteady solution is a small linear perturbation about some nonlinear steady state solution. In other words, the unsteady solution is linearized with respect to time.

Equation 3 has the advantage that ϕ_1 can be computed using essentially the same well-known finite-difference relaxation algorithms used to compute the mean steady state solution ϕ_0. Based on this approach, Traci et al.

12

(Reference 13) developed computer programs STRANS2 and UTRANS2 that can solve the steady and unsteady aerodynamic equations, respectively. Because of the elliptic/hyperbolic characteristic of the governing equations for the steady and unsteady perturbation velocity potentials, the mixed differencing line relaxation procedure of Murman and Cole was used for steady and unsteady computations. These programs are used in the present report to compute aerodynamic data for flutter analysis.

2.3 Time Integration Method

In the harmonic method, a time linearized assumption is used to obtain the unsteady solution. Such method constrains the shock wave to its steady-state position. As an alternative and more complete solution, Ballhaus and Goorjian (Reference 14) proposed to use the time integration method to obtain an unsteady transonic solution. In this method, the shock movements can accurately be treated. Also, there is no need to linearize the aerodynamic equations with respect to time in the unsteady part.

As a further simplification of Equation 1, the frequency of the transonic flow can be assumed as low so that $k_c \simeq 1 - M_\infty^2 \simeq \tau^{2/3} \ll 1$. Equation 1 may then be reduced to

$$2k_c M_\infty^2 \phi_{xt} = V_c \phi_{xx} + \phi_{yy} \qquad (4)$$

where τ is the thickness-chord ratio of the airfoil.

Equation 4 is suitable for the time integration approach. This approach is based on the finite difference scheme that integrates Equation 2 in time for harmonic aerodynamic motions until the transient states in the solution disappear and the forces become periodic.

Several numerical procedures are available to solve Equation 4. Among them

13

the procedure developed by Ballhaus and Goorjian (Reference 14) based on the
alternate-direction implicit algorithm has been proven to be computationally
efficient and is being widely used. This procedure uses a conservative,
implicit finite-difference scheme to time-accurately integrate the nonlinear,
low-frequency,transonic small-disturbance equation as defined in Equation 4.
A computer code LTRAN2 was developed based on this procedure. This code can
be used to find the flow field solutions for airfoils with arbitrary
combinations of pitch, plunge,and flap deflections.

In order to comply with the low-frequency approximation of LTRAN2, the
unsteady aerodynamic coefficients were computed for a reduced frequency range
$k_c \leq 0.2$.

Although UTRANS2 retains the ϕ_{tt}-term, it experiences numerical instability
difficulty at higher reduced frequencies. Hence, in this study the reduced
frequencies considered for UTRANS2 were also limited to the range $k_c \leq 0.2$.

14

SECTION III

AEROELASTIC AND TRANSFORMATION EQUATIONS

In the present flutter analysis, the airfoil is assumed to oscillate about the elastic axis with two degrees of freedom, plunge and pitch. The necessary aeroelastic equations of motion and the transformation equations for aerodynamic coefficients are discussed in this section.

3.1 Aeroelastic Equations of Motion

The parameters and sign conventions for a typical airfoil oscillating with pitching and plunging degrees of freedom are defined in Figure 1. The following assumptions are made in deriving the equations:

(1) The displacement h and rotation α are measured with respect to the mean position, defined by the steady state conditions.

(2) The airfoil is rigid.

(3) The amplitudes of oscillation are small.

(4) The principle of superposition for aerodynamic forces is valid even in the presence of shocks. Discussion and justification of this assumption were given in References 12 and 15.

Considering the inertia forces, elastic forces, and aerodynamic forces, the equations of motion are

$$\begin{cases} Q_h = m\ddot{h} + S\ddot{\alpha} + k_h h \\ Q_\alpha = S\ddot{h} + I_\alpha\ddot{\alpha} + k_\alpha\alpha \end{cases} \tag{5}$$

or

15
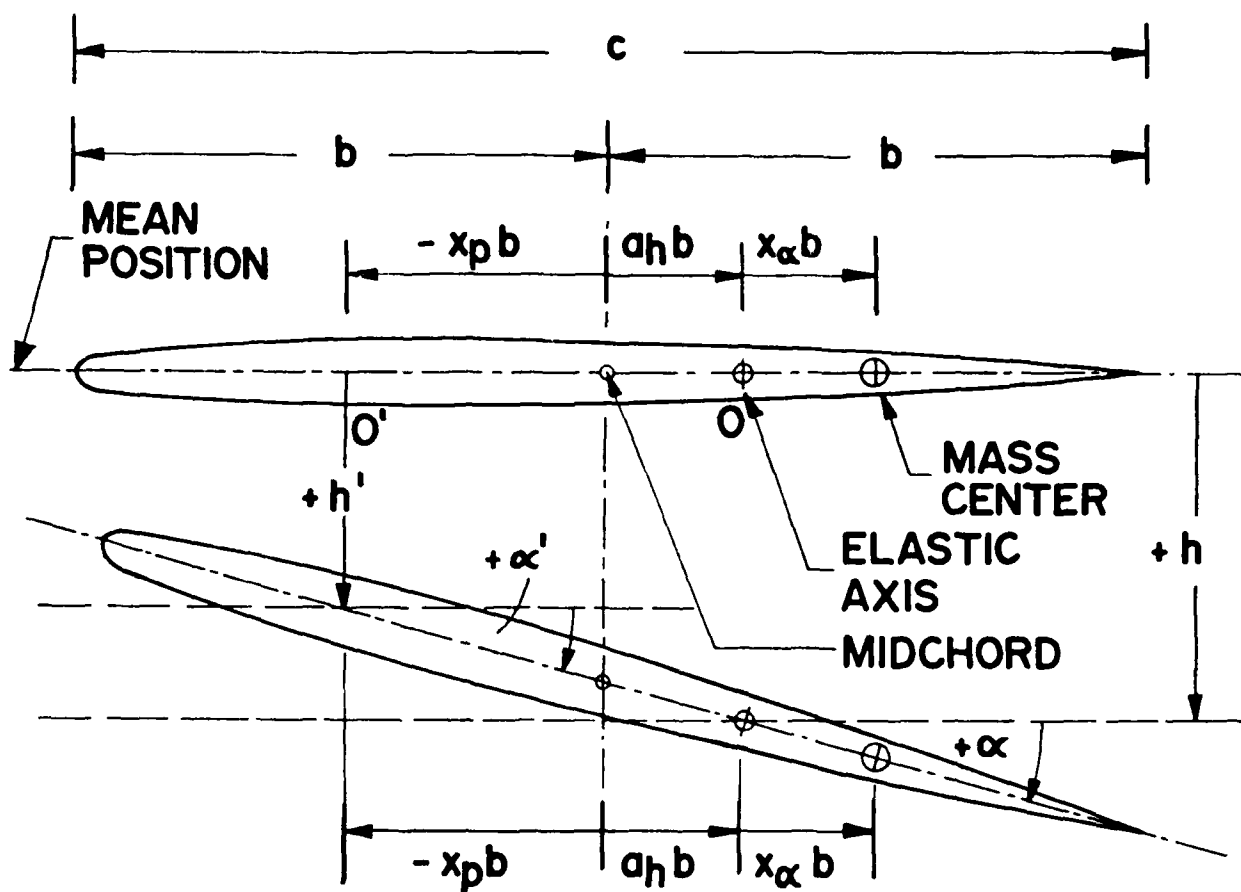
Figure 1.   Definition of Parameters for Two - D.O.F. Aeroelastic System

16

$$\begin{cases} \ddot{\xi} + x_\alpha \ddot{\alpha} + \xi \omega_h^2 = Q_h/mb \\ x_\alpha \ddot{\xi} + r_\alpha^2 \ddot{\alpha} + r_\alpha^2 \omega_\alpha^2 \alpha = Q_\alpha/mb^2 \end{cases} \tag{6}$$

where $\xi = h/b$; $\omega_h = (k_h/m)^{1/2}$; $x_\alpha = S/mb$; $\omega_\alpha = (k_\alpha/I_\alpha)^{1/2}$ and $r_\alpha = (I_\alpha/mb^2)^{1/2}$.

Structural damping can be introduced into Equations 6 by replacing ω_h^2 and ω_α^2 by $\omega_h^2(1 + g_h)$ and $\omega_\alpha^2(1 + g_\alpha)$, respectively. The damping coefficients g_h and g_α correspond to plunging and pitching modes, respectively. It is further assumed that g_h and g_α are small and of the same order.

Assuming harmonic oscillations with flutter frequency ω and expressing the aerodynamic forces Q_h and Q_α in terms of aerodynamic coefficients $C_{\ell\delta}$, $C_{\ell\alpha}$, $C_{m\delta}$, and $C_{m\alpha}$, Equations 6 yield the final eigenvalue equations for flutter analysis as

$$[\mu k_b^2 [M] - [A]] \begin{Bmatrix} \xi_0 \\ \alpha_0 \end{Bmatrix} = \lambda [K] \begin{Bmatrix} \xi_0 \\ \alpha_0 \end{Bmatrix} \tag{7}$$

where ξ_0 and α_0 are the nondimensional amplitudes in plunge and pitch oscillations, respectively; $\mu = m/\pi \rho b^2$, the airfoil-air mass ratio; $k_b = \omega b/U$, the reduced frequency.

The matrices [M], [A], and [K] are defined as

$$[M] = \begin{bmatrix} 1 & x_\alpha \\ \hline x_\alpha & r_\alpha^2 \end{bmatrix} \tag{8a}$$

$$[A] = \frac{1}{\pi} \begin{bmatrix} C_{\ell\delta}/2 & C_{\ell\alpha} \\ \hline -C_{m\delta} & -2C_{m\alpha} \end{bmatrix} \tag{8b}$$

17

$$[K] = \begin{bmatrix} (\omega_h/\omega_r)^2 & 0 \\ \hline 0 & r_\alpha^2(\omega_\alpha/\omega_r)^2 \end{bmatrix} \qquad (8c)$$

The eigenvalue λ is a complex number defined as

$$\lambda = \mu(1 + ig)\omega_r^2 b^2/U^2 \qquad (9)$$

where $g = g_h = g_\alpha$ is the structural damping coefficient which is assumed to be small and of the same order for both plunging and pitching modes. The flutter solution is obtained when g is found to be zero. In the transonic flutter analysis, to compute the aerodynamic coefficients for Equation 8b comprises the essential task.

3.2 Transformation of Aerodynamic Coefficients

In obtaining the aerodynamic coefficients, it is a common practice to pitch the airfoil about the elastic axis so that such coefficients can be directly used to compute the aerodynamic matrix [A] in Equation 8b. But in some situations this may not be the case. For example, the position of the elastic axis is considered to be a variable in this paper so that its effect on flutter characteristics can be studied. Thus the aerodynamic coefficients originally obtained with reference to a pitching axis must be transformed to those with reference to the elastic axis for aeroelastic analysis. The transformation relations can be derived by using the principle of superposition of airloads.

Let it be assumed that the aerodynamic coefficients $C'_{\ell\delta}$, $C'_{\ell\alpha}$, $C'_{m\delta}$, and $C'_{m\alpha}$ for point O' (see Fig. 1) due to pitching about O' have been obtained. It is desired to transform these coefficients to be $C_{\ell\delta}$, $C_{\ell\alpha}$, $C_{m\delta}$, and $C_{m\alpha}$ for another

13

pitching axis (elastic axis) 0.

Assuming rigid airfoil and small amplitude of oscillations, the transformation relationships may be written as

$$C_{\ell\delta} = C_{\ell\delta}'$$

$$C_{\ell\alpha} = C_{\ell\alpha}' - (sC_{\ell\delta}')$$

$$C_{m\delta} = C_{m\delta}' + sC_{\ell\delta}'$$

$$C_{m\alpha} = C_{m\alpha}' + sC_{\ell\alpha}' - (sC_{m\delta}') - (s^2C_{\ell\delta}')$$

(10)

where $s = (a_h - x_p)/2$. The three terms in the parentheses are relatively small when compared with the other terms. If they are neglected, Equations 10 are in the form as those given previously by Traci et al. in Reference 13.

SECTION IV

PROCEDURES OF OBTAINING AERODYNAMIC DATA

The steady and unsteady aerodynamic data were obtained by both time integration and harmonic method by using LTRAN2 and STRANS2/UTRANS2, respectively. In this section, the finite difference grids used and other salient features of the procedure for obtaining the aerodynamic data are discussed.

4.1 Method of Obtaining Aerodynamic Data from LTRAN2

4.1.1 Finite Difference Computational Grid

The size and the pattern of the grid play an important role in obtaining accurate results from LTRAN2. Because of the various reasons discussed in Reference 14, a fairly fine mesh is required in order to obtain acceptable solutions. However, the mesh size is often limited by the capacity of the core memory in the available computer.

In this analysis, a 79 x 99 finite difference mesh, with 79 grid points in the vertical (y) direction and 99 grid points in horizontal (x) direction, was employed for final computations. Details of this grid were supplied by Ballhaus and Goorjian. This was the finest grid size that could be practically used on the CDC 6500 computer available at Purdue University.

This grid has a smooth, nonuniform pattern and it is symmetric about the y = 0 line. The spacings of the grid points are smaller near the leading and trailing edges in x-direction and near the mean chord line in the y-direction. The spacings are gradually enlarged as the grid points are farther away from the airfoil. Thus the grid boundaries are located sufficiently away from the airfoil both in x- and y-directions. From leading edge to trailing edge, a

20

total of 33 grid points is used so that an accurate representation of the pressure distribution can be obtained, particularly when there is a shock. Other salient features for this grid are given as follows:

(1) Minimum spacing in x-direction = 0.0033c

(2) Minimum spacing in y-direction = 0.02c

(3) Distance between the upstream grid boundary and the leading edge = 1033.53c

(4) Distance between the downstream grid boundary and the leading edge = 855.91c

(5) Distance between the upper or lower grid boundary and the mean chord line = 811.12c.

4.1.2 Steady-State Computations

The steady-state solution is required as an initial condition for the unsteady computations. In this analysis, the steady-state solution was obtained by using the successive line over-relaxation method (SLOR) available in the LTRAN2 code.

In the process of obtaining the steady-state solution, multiple grid computations were carried out in order to accelerate the rate of convergence. First, a converged steady-state solution was obtained for a coarse grid (35x38). This solution was then interpolated to form a starting solution for a medium grid (53x79). A converged solution was then obtained for the medium grid. This solution was again interpolated to form a starting solution for the final computational grid (79 x 99).

The SLOR computations were carried out for the fine grid (79x99) for several hundred iterations. This iterative process was stopped when the

21

variation in the perturbation velocity potential at all grid points between consecutive iterations reached a value of about 1×10^{-5}. This process required about 1200 iterations. The steady solution obtained at this stage was used to plot the pressure curves and also used as a starting solution for the unsteady computations.

4.1.3 Unsteady Computations

Steady-state results obtained by the SLOR method were used as the initial conditions for unsteady computations. In order to obtain unsteady results, the airfoil was first subjected to a harmonic forced motion. In all the cases, the angle of attack α was varied sinusoidally with an amplitude of 0.5° and the aerodynamic equation was integrated in time by LTRAN2. During the process of time integration, 240 time steps per cycle were used. After some duration of time, the effect of the initial conditions on the unsteady solution became negligible such that the aerodynamic force coefficients C_{ℓ} and C_m became periodic. In general, four to six cycles of forced motion were required to obtain fairly periodic results from LTRAN2. At this stage, the amplitudes and phase angles of the aerodynamic force coefficients $C_{\ell\alpha}$ and $C_{m\alpha}$ were computed.

The plunging oscillations were treated as a special case of pitching oscillations. The plunging oscillations can be presented by an oscillation of induced angle of attack by using the relations $\alpha_i = \dot{h}/U$, where α_i represents the induced angle of attack, $\dot{h}$ represents the rate of change of plunging displacement, and U is the flight speed. The unsteady aerodynamic coefficients $C_{\ell\delta}$ and $C_{m\delta}$ were obtained by the same procedure described above as that used to obtain $C_{\ell\alpha}$ and $C_{m\alpha}$. This was carried out by replacing the sinusoidal variation of angle of attack α by the sinusoidal variation of induced angle of attack α_i.

22

4.2 Method of Obtaining Aerodynamic Data from STRANS2 and UTRANS2

4.2.1 Finite Difference Computational Grid

Within the contraints of accuracy, efficiency, and computer core memory, a 71x74 finite difference mesh was chosen with 71 grid points in the vertical (y) direction and 74 grid points in horizontal (x) direction.

The grid is smoothly nonuniform with symmetry about the mean chord line. In x-direction, the grid points are distributed more densely at:(i) the leading edge to account for the blunt nose; (ii) the expected shock-position to more precisely capture the shock; and (iii) the trailing edge for better application of the Kutta-condition. In y-direction, the grid points are more closely spaced near the mean chord line. The grid spacing is gradually widened as the grid points move away from the airfoil and towards the boundaries. The grid boundaries are sufficiently far from the airfoil to reduce flow interaction between the airfoil and the boundaries to a minimum. The grid has the following specific features:

(1) Total points on the airfoil = 37

(2) Number of grid points between the upstream grid boundary and the leading edge = 21

(3) Minimum spacing in x-direction = 0.0025c

(4) Minimum spacing in y-direction = 0.01c

(5) Distance between the upstream grid boundary and the leading edge = 4c

(6) Distance between the downstream grid boundary and the leading edge = 4c

(7) Distance between the upper or lower grid boundary and the mean chord line = 8c.

4.2.2 Steady-State Computations (STRANS2)

This method, too, requires the steady-state solution as input for the unsteady calculations. For the computation of the steady-state solution a mixed differencing relaxation procedure introduced by Murman and Cole is used in STRANS2.

The relaxation parameters used were -0.75 for parabolic (sonic) and hyperbolic (supersonic) grid points, and 1.7 for elliptic (subsonic) grid points.

The airfoil calculation in the farfield was updated every 40 iterations with a relaxation parameter of 1.5.

To expedite convergence, a built-in grid refinement scheme was used. First, a coarse grid of 37x39 grid-points was converged to the point where the difference in steady perturbation velocity potential at all grid points between two consecutive iterations (the tolerance) was less than 1×10^{-4}. This solution was then used as a starting input for a finer grid of 71x74 grid points. The convergence tolerance for the fine grid was chosen to be 1×10^{-5}. This was achieved in about 700 iterations.

4.2.3 Unsteady Computations (UTRANS2)

The unsteady computer code UTRANS2 needs the steady-state results as input for the unsteady computations. The unsteady solutions are obtained by using the same parameters and the same mixed differencing relaxation procedure as in the steady computations.

The moderate frequency approach, incorporating the ϕ_{tt}-term in the full potential equation and in the boundary conditions, was used for all unsteady computations. Again, the grid-refinement procedure was used to expedite the convergence. The same convergence tolerances were used. This was achieved in

24

400 iterations to 2400 iterations, depending on the Mach number and reduced frequency. In general, the number of iterations increases with increase in angle of attack, Mach number, and reduced frequency. Also the pitch computations took more iterations to converge than the plunge computations.

SECTION V

RESULTS

Flutter analyses were carried out for three airfoil configurations: (1) a MBB A-3 supercritical airfoil; (2) a MBB A-3 airfoil with camber removed; and (3) a NACA 64A010 airfoil scaled down to 8.9% maximum thickness-to-chord ratio, the same as that of airfoil 1. All airfoils were assumed to oscillate with two degrees of freedom, plunge and pitch about the elastic axis.

Airfoil 1 was first analyzed for design Mach number $M_\infty = 0.765$ and $\alpha = 0^o$ by both methods. It was then analyzed for the design Mach number and the design lift coefficient $C_\ell = 0.58$. Two different equivalent design angles of attack had to be used for the two different methods in order to produce the same value $C_\ell = 0.58$.

To investigate the effect of camber and thickness distribution on the supercritical airfoil design, airfoils 2 and 3 were analyzed at $M_\infty = 0.765$ and the equivalent design angles of attack. Finally, the effect of Mach number on flutter speed (the transonic dip phenomenon) was studied for airfoil 1 at zero mean angle of attack.

5.1 Configuration of the MBB A-3 Supercritical Airfoil

In order to perform accurate aerodynamic computations, it is necessary to use accurate data for the airfoil configurations, especially in the region of the leading edge. The equations for accurate curve fitting and tabulated data for eight AGARD/SMP standard airfoil configurations were provided by Dr. J.J. Olsen of the Flight Dynamics Laboratory (Reference 19).

The equations for the eight airfoil configurations were given by Dr. Olsen

26

as

$$\left\{ \begin{array}{l} Z_u(x) = c(x) + 0.5\ t(x) \\[1em] Z_\ell(x) = c(x) - 0.5\ t(x) \\[1em] t(x) = a_0\sqrt{x} + a_1 + a_2 x + a_3 x^2 + a_4 x^3 + a_5 x^4 \\[1em] c(x) = \qquad\ \ b_1 + b_2 x + b_3 x^2 + b_4 x^3 + b_5 x^4 \end{array} \right. \qquad (11)$$

where $Z_u(x)$ and $Z_\ell(x)$ are the equations for the upper and lower surfaces, respectively; x is the nondimensional axis with leading edge at x = 0 and trailing edge at x = 1; $c(x)$ is the function of camber; $t(x)$ is the function of thickness; and constants a's and b's for the eight airfoils are available in Reference 19.

The coefficients for the thickness function for the MBB A-3 airfoil are: a_0 = 0.2457807; a_1 = 0; a_2 = - 0.2470393; a_3 = 0.5556936; a_4 = -1.1377743; and a_5 = 0.5833393. The coefficients for the camber function are: b_1 = 0; b_2 = 0.1294408; b_3 = -0.4206819; b_4 = 0.5516741; and b_5 = -0.2604330. A plot of this configuration is given in Figure 2.

The MBB A-3 airfoil configuration without camber is also plotted in Figure 2. It is obtained by setting the coefficients of the camber function to zero in Equation 11. The coefficients for the thickness function remain the same.

In order to compare the effect of thickness distribution on flutter behavior between a supercritical and an equivalent conventional design, the configuration of a NACA 64A010 airfoil was scaled down in thickness by 11%. This is done by multiplying the coefficients in the thickness function for the NACA 64A010 airfoil by 0.89. The values of those coefficients for the NACA 64A010 airfoil are available in Reference 19. They are: a_0 = 0.2255645; a_1 = 0; a_2 = -0.0699163; a_3 = 0.0664236; a_4 = -0.541599; and a_5 = 0.3199472.

27
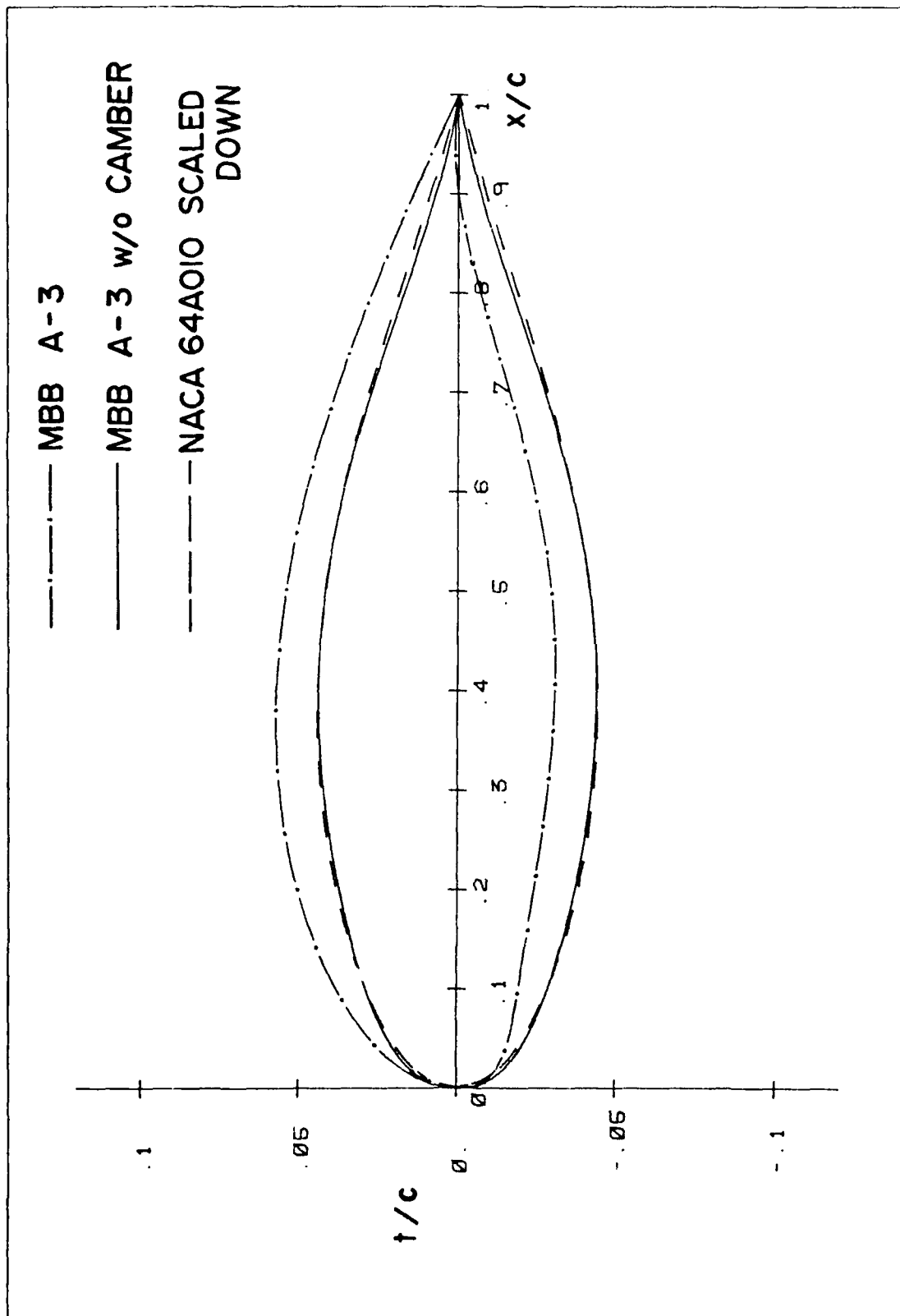
Figure 2. Configurations for MBB A-3 Airfoil, MBB A-3 Airfoil without Camber, and NACA 64A010 Airfoil Scaled Down to 8.9" Maximum Thickness - Chord Ratio.

This airfoil has no camber.

It is obvious in Figure 2 that the profile of the MBB A-3 supercritical airfoil becomes considerably different when the camber is removed. It can naturally be expected that the camber has an obvious effect on the aerodynamic and flutter results. On the other hand, the profile of the MBB A-3 airfoil without camber is quite similar to that of the scaled down model of the NACA airfoil. Thus an obvious difference in aerodynamic and flutter results between the two profiles may not be expected.

5.2 Flutter Analysis of the MBB A-3 Supercritical Airfoil at $M_\infty = 0.765$ and $\alpha = 0°$.

The MBB A-3 supercritical airfoil was designed for $M_\infty = 0.765$ and $\alpha = 1.3°$ which yield a lift coefficient of $C_\ell = 0.58$. A case with zero angle of attack at design Mach number was first considered. Based on this case, a comparison between the two computer programs (STRANS2/UTRANS2 and LTRAN2) can be made. Furthermore, the results can provide a comparative basis for the case with angle of attack.

5.2.1 Steady Pressure Curves

The steady pressure curves obtained at $M = 0.765$ and $\alpha = 0.0°$ by both LTRAN2 and STRANS2 are shown in Figure 3.

Both programs predicted a shock on the upper surface. LTRAN2 gives a stronger shock than STRANS2. The shock location obtained by LTRAN2 is behind that obtained by STRANS2. However, the agreement in lower surface pressure between the two programs is excellent. The discrepancies in the upper surface pressure curves between the two programs may be due to the difference in the finite difference mesh and due to the difference in the shock capturing technique.

29
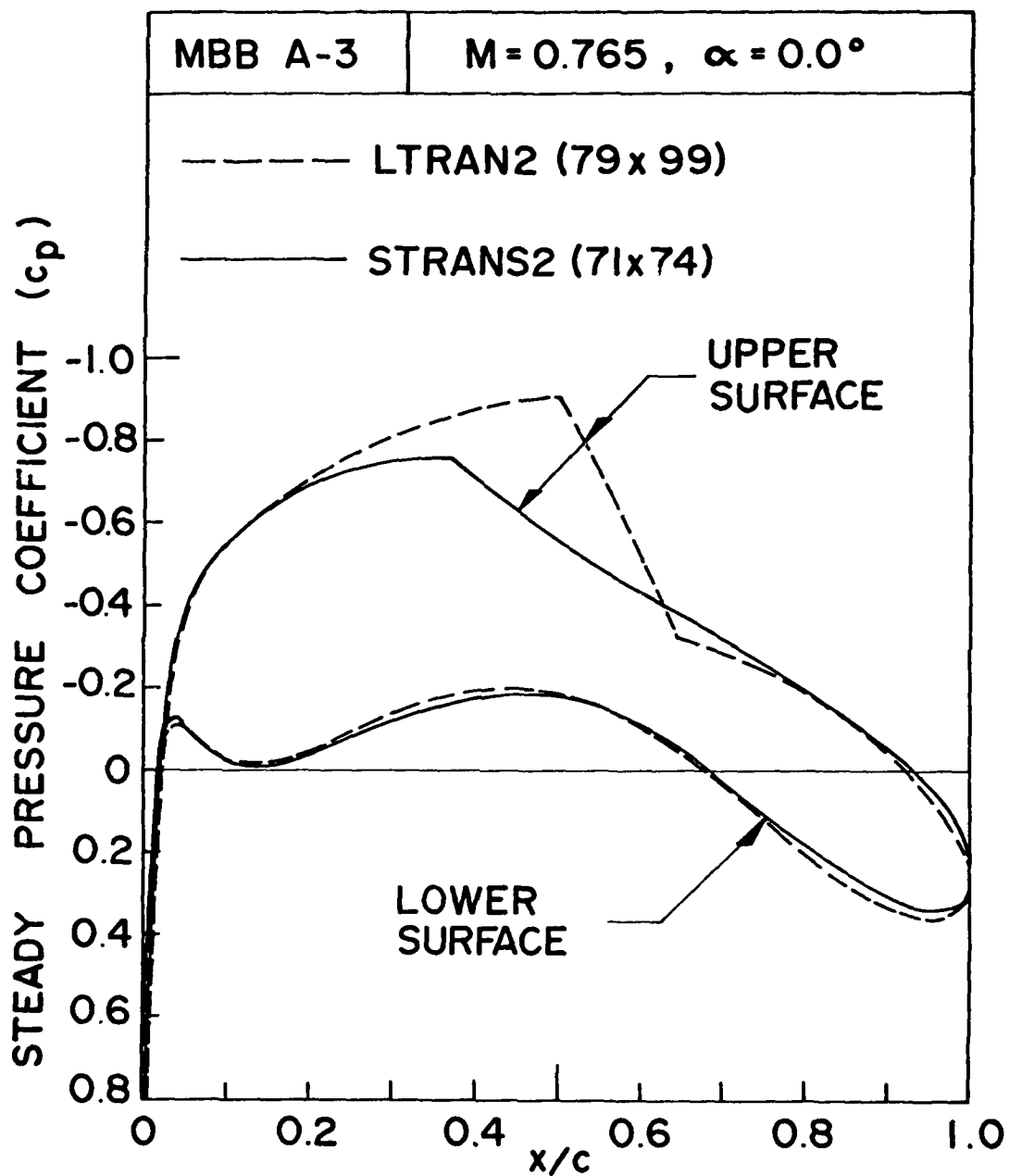
Figure 3. Distribution of Steady Pressure Coefficients for MBB A-3 Airfoil at M = 0.765 and α = 0.0°.

5.2.2 Unsteady Aerodynamic Coefficients

The MBB A-3 airfoil was assumed to oscillate with two degrees of freedom, plunge and pitch about the quarter-chord axis. Consequently, four unsteady aerodynamic coefficients were computed: the lifting force coefficient due to unit plunging displacement $c_{\ell\delta}$; the lifting force coefficient due to unit pitching rotation $c_{\ell\alpha}$; the moment coefficient due to unit plunging displacement $c_{m\delta}$; and the moment coefficient due to unit pitching rotation $c_{m\alpha}$. All four coefficients were obtained by assuming that the airfoil was pitching about the quarter-chord at M = 0.765 with zero mean angle of attack.

Table 1 shows the unsteady aerodynamic coefficients obtained by using both harmonic method (UTRANS2) and time integration method (LTRAN2). Reduced frequencies considered were 0.0, 0.05, 0.10, 0.15, and 0.20 for UTRANS2 and 0.05, 0.10, 0.15, and 0.20 for LTRAN2, respectively.

The coefficients obtained by the two programs show similar general trend. Reasons for some differences may be attributed to: (1) the basic difference in the steady pressure curves; (2) different assumptions used in the methods; (3) different finite difference schemes for unsteady flow computation.

The level of agreement for the moment coefficients is not as good as that for the lift coefficients. This may be due to the fact that the lift coefficients were obtained by merely integrating the area under the unsteady pressure curves whereas the moment coefficients were obtained by integrating the area-moment under the unsteady pressure curves. The former integration results in less error than the latter. However, it was found during the flutter analysis that such differences do not appear to significantly affect the agreement in flutter results. Such finding was reported earlier in Reference 12.

Table 1 Aerodynamic Coefficients for MBB A-3 Airfoil at M = 0.765
and $\alpha = 0.0^0$

	Method	Reduced Frequency (k_c)									
		0.0		0.05		0.10		0.15		0.20	
		Real	Imag.	Real	Imag.	Real	Imag.	Real	Imag.	Real	Imag.
C_{ℓ_δ}	1	0.0	0.0	0.171	0.636	0.422	1.100	0.724	1.420	0.881	1.728
	2	0.0	0.0	0.089	0.521	0.260	0.900	0.523	1.185	0.772	1.288
C_{ℓ_α}	1	-	-	12.724	-3.409	11.001	-4.223	9.469	-4.825	8.642	-4.403
	2	11.221	0.0	10.141	-1.949	8.843	-2.801	7.667	-3.060	6.710	-2.970
C_{m_δ}	1	0.0	0.0	-0.008	-0.038	-0.015	-0.071	-0.022	-0.103	-0.029	-0.136
	2	0.0	0.0	0.003	-0.015	0.010	-0.031	0.017	-0.053	0.020	-0.076
C_{m_α}	1	-	-	-0.763	0.162	-0.706	0.150	-0.686	0.146	-0.680	0.145
	2	-0.311	0.0	-0.307	-0.074	-0.319	-0.148	-0.340	-0.212	-0.365	-0.265

Method 1: Time Integration   (79x99)   LTRAN2
Method 2: Harmonic Analysis   (71x74)   UTRANS2

5.2.3 Flutter Results

The flutter results were computed by standard U-g method described in Reference 12. Flutter speeds and corresponding reduced frequencies were obtained by varying one of the four aeroelastic parameters: airfoil-air mass ratio μ; position of the mass center x_α; position of the elastic axis a_h; and plunge-pitch frequency ratio ω_h/ω_α. In all cases, the values of the radius of gyration r_α and the reference frequency ω_r were assumed as 0.5 and 1.0, respectively.

Figure 4 shows the curves for flutter speed and corresponding reduced frequency versus the location of the mass center x_α for the MBB A-3 super-critical airfoil pitching about the quarter-chord. The airfoil-air mass ratio μ was assumed as 100. The plunge-to-pitch frequency ratios ω_h/ω_α were assumed as 0.1, 0.2, 0.3, and 0.4, respectively.

In Figure 4, flutter speed is seen to decrease as the mass center moves from the elastic axis toward the mid-chord. It increases very sharply as the mass center approaches the elastic axis. The curves drop as ω_h/ω_α increases. The curves for the reduced frequency demonstrate a behavior opposite to that of the flutter curves.

The curves obtained by the two methods agree quite well both in trend and magnitude. The poor agreement in the very low range of x_α is due to the sharp increase in flutter speed.

The curves in Figure 5 show the effect of airfoil-air mass ratio μ on the flutter speed and the corresponding reduced frequency for the MBB A-3 airfoil. The mass center was assumed to be at 3/8-chord ($x_\alpha = 0.25$). The values of reduced frequency considered were 0.1, 0.2, and 0.3, respectively.

The curves obtained by both methods are in quite reasonable agreement

Figure 4. Effect of Position of Mass Center on Flutter Speed for Various Plunge-
to-Pitch Frequency Ratios for MBB A-3 Airfoil at M = 0.765 and α = 0.0°.

34

Figure 5. Effect of Airfoil-Air Mass Ratio on Flutter Speed for Three Plunge-to-Pitch Frequency Ratios for MBB A-3 Airfoil at M = 0.765 and α = 0.0°.

35

both in trend and in value of flutter speed. Within the range of values considered for μ and ω_h/ω_α, it is seen that the flutter speed increases as μ increases and also increases as ω_h/ω_α decreases. The curves for reduced frequency demonstrate a trend reverse to that of the curves for flutter speed.

Figure 6 shows the effect of the position of the elastic axis on flutter results. Since all the aerodynamic coefficients were obtained by pitching the airfoil about the 1/4-chord axis ($a_h = - 0.5$), it was necessary to use the transformation Equation 10 when a_h was varied. The mass center was fixed at 3/8-chord and the airfoil-air mass ratio was set equal to 100. Frequency ratios considered were 0.1, 0.2, 0.3, and 0.4, respectively.

In Figure 6, the flutter speed increases as the elastic axis moves toward the mid-chord. Such increasing trend becomes less obvious for lower frequency ratios. When the mass center approaches the elastic axis ($x_\alpha = 0$) the flutter speed becomes independent of the frequency ratio. This phenomenon was observed when analysis was made for a NACA 64A006 airfoil and a simple explanation was given in Reference 20.

The curves obtained by both methods are in reasonably good agreement.

5.3 Flutter Analysis of the MBB A-3 Supercritical Airfoil at $M_\infty = 0.765$
      and $C_\ell = 0.58$

The MBB A-3 supercritical airfoil was designed to give a steady lift coefficient $C_\ell = 0.58$ at $M_\infty = 0.765$ and $\alpha = 1.3^o$. It was found that the angles of attack required to obtain $C_\ell = 0.58$ at $M_\infty = 0.765$ are 0.42^o and 0.75^o for LTRAN2 and STRANS2, respectively. These two angles of attack were used for the two respective programs in this section. Consequently, it becomes less meaningful to compare the two sets of results obtained by assuming two different angles of attack.
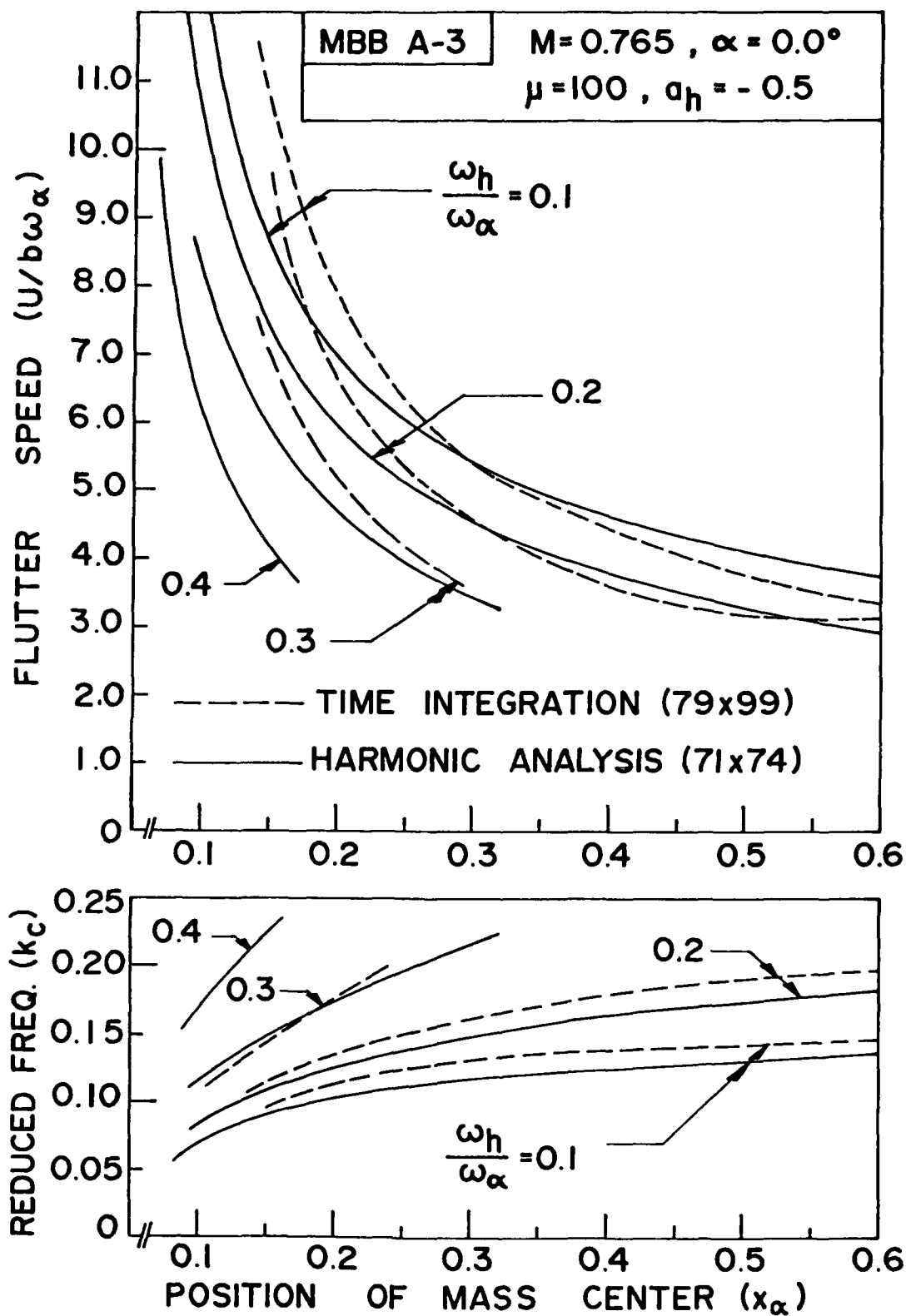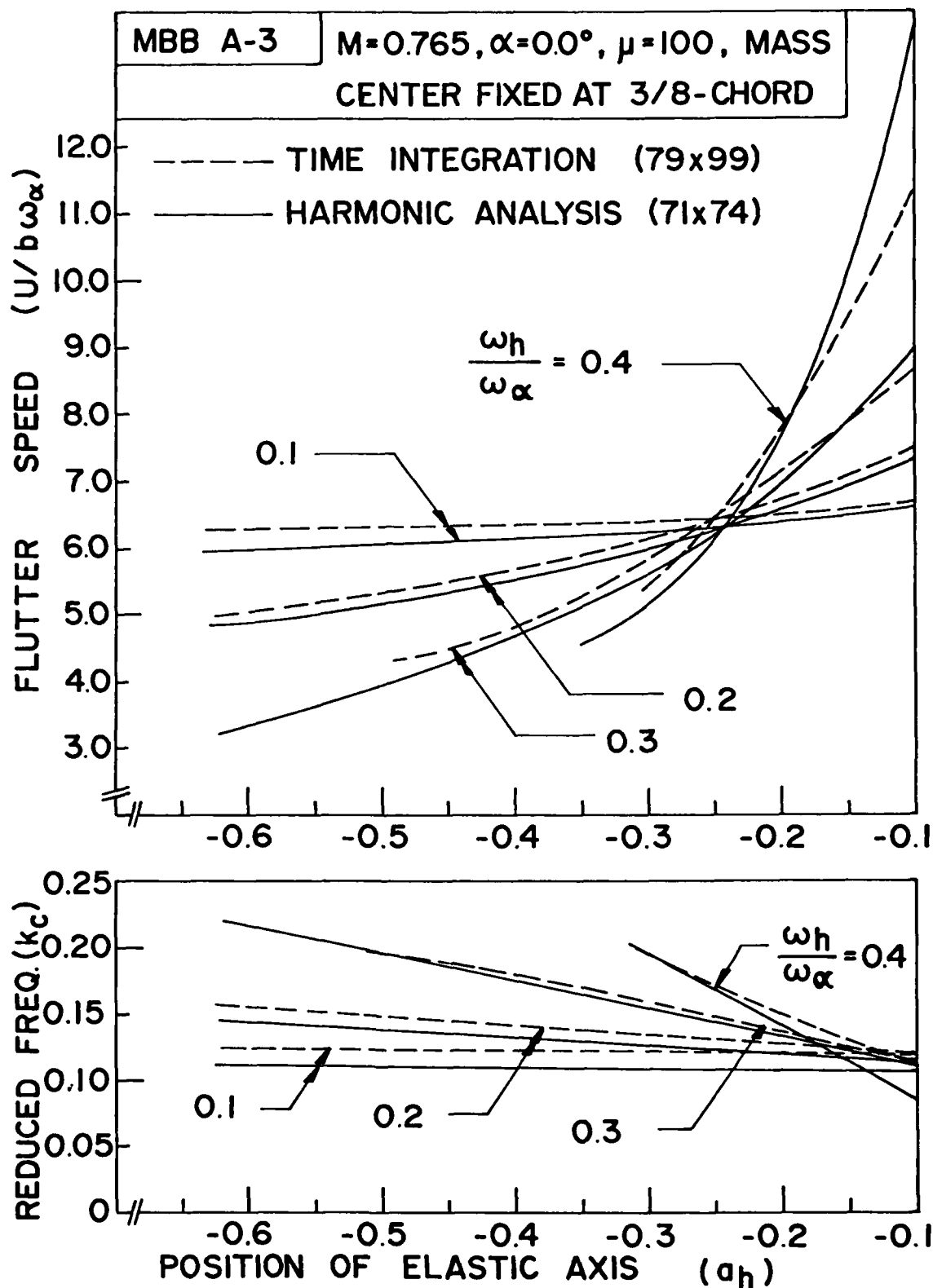
Figure 6. Effect of Position of Elastic Axis on Flutter Speed for Various Plunge-
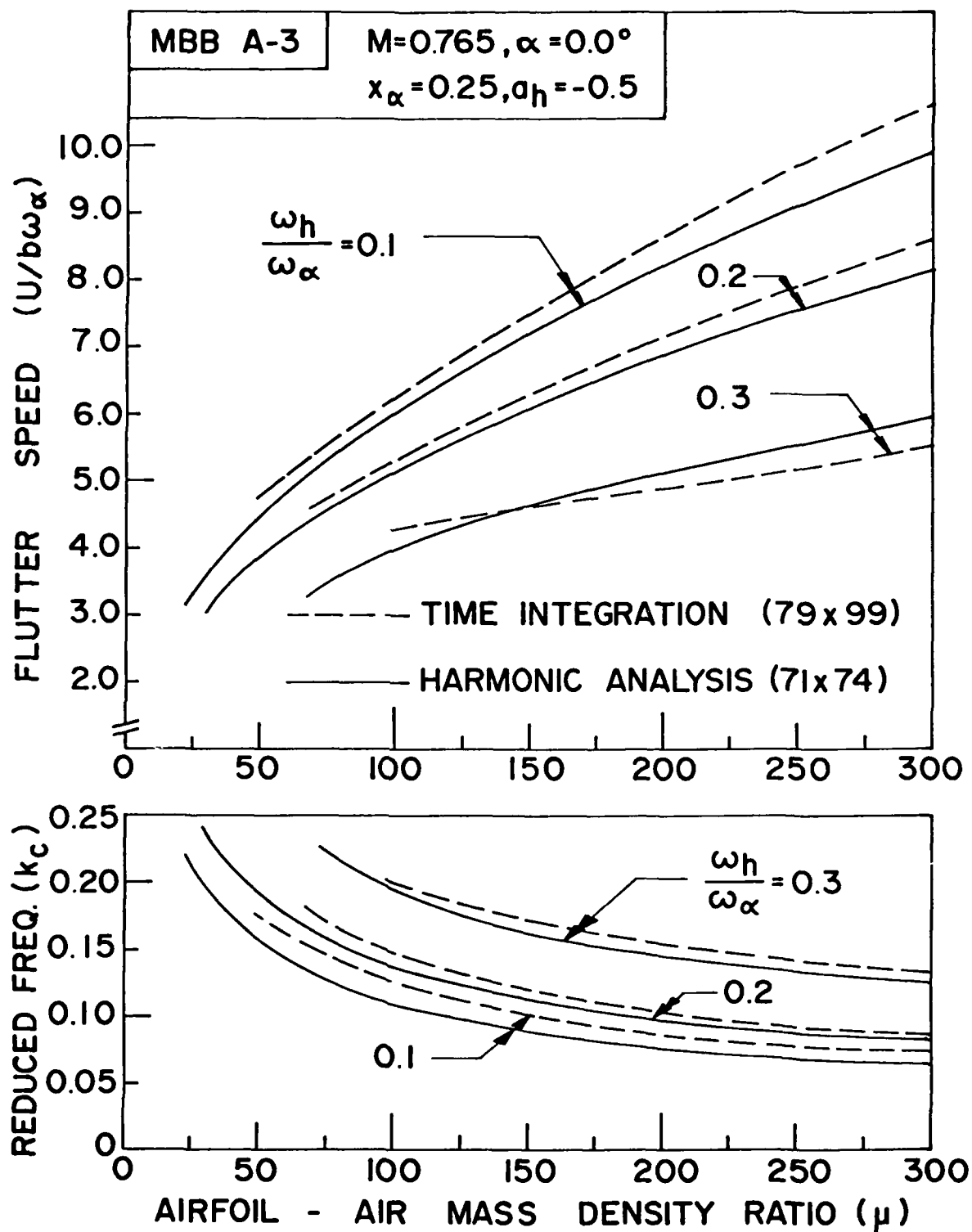to-Pitch Frequency Ratios for MBB A-3 Airfoil at M = 0.765 and α = 0.0°.

37

5.3.1 Steady Pressure Curves

Figures 7 and 8 show the steady pressure curves for the MBB A-3 airfoil at $M_\infty = 0.765$ obtained from LTRAN2 ($\alpha = 0.42^O$) and STRANS2 ($\alpha = 0.75^O$), respectively. In both figures, the pressure curves for $\alpha = 0^O$ are also shown for comparison.

Both figures show that the equivalent design angles of attack have the following effects: (1) The shocks become stronger and move toward the trailing edge; (2) The pressure curves on the upper surface show more negative pressure area; (3) The pressure curves on the lower surface show less negative pressure area. Such effects result in an increase in lift coefficients.

5.3.2 Unsteady Aerodynamic Coefficients

Based on the steady pressure coefficients obtained in Figures 7 and 8, the corresponding unsteady aerodynamic coefficients were obtained and given in Tables 2 and 3, respectively. In both tables, corresponding coefficients obtained for the special case $\alpha = 0^O$ are also given for comparison.

Tables 2 and 3 show that the magnitudes of the lift and moment coefficients are higher in the two cases of equivalent design angles of attack. The increases are more pronounced in moment coefficients than in lift coefficients. Such increases may be due to the stronger shocks which occurred in the two cases of equivalent design angles of attack.

5.3.3 Flutter Results

Figures 9 and 10 show the effect of the position of mass center on the flutter results obtained by use of the time integration method (LTRAN2) and the harmonic method (UTRANS2), respectively. In both figures, curves for flutter speed are plotted for several values of ω_h/ω_α. The values for μ and a_h were
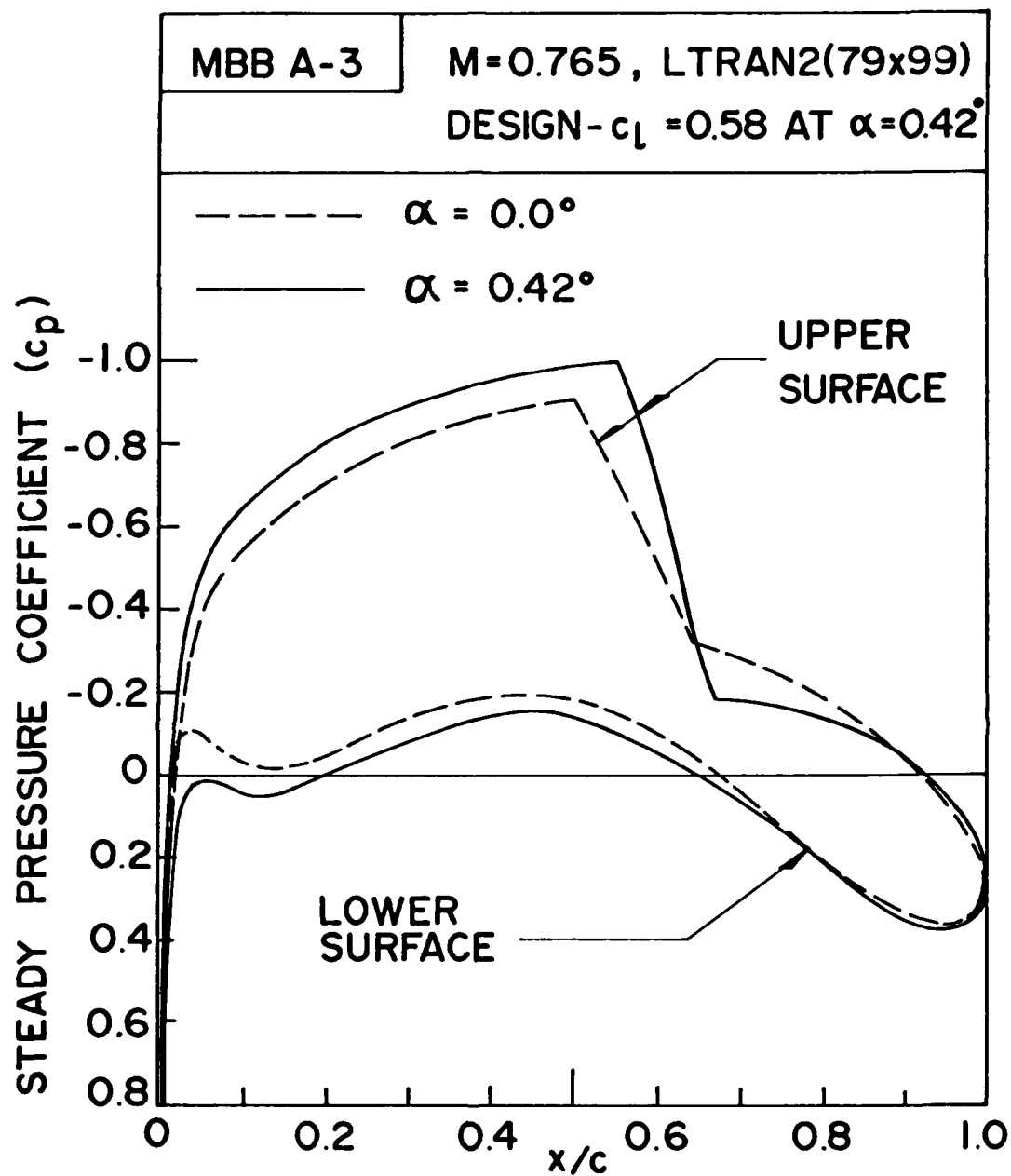
Figure 7. Distribution of Steady Pressure Coefficients for MBB A-3 Airfoil at M = 0.765 and α = 0.0[o] and 0.42[o] (by LTRAN2).
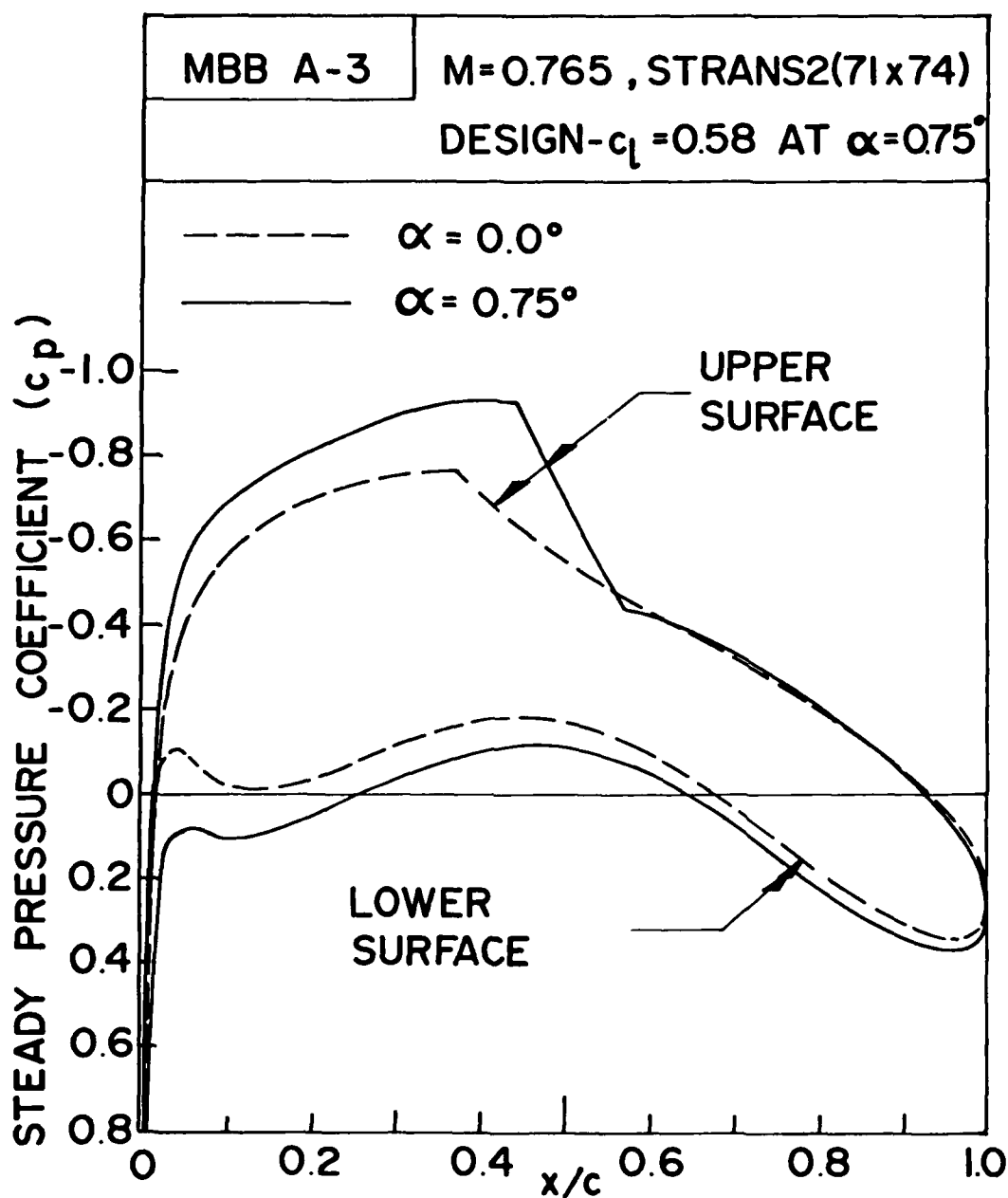
Figure 8. Distribution of Steady Pressure Coefficients for MBB A-3 Airfoil at M = 0.765 and α = 0.0° and 0.75° (by STRANS2).

Table 2 Aerodynamic Coefficients for MBB A-3 Airfoil at M = 0.765, and α = 0.0° and α = 0.42° by Time Integration (LTRAN2) with 79x99 – Grid

	Angle, α	Reduced Frequency (k_c)							
		0.05		0.10		0.15		0.20	
		Real	Imag.	Real	Imag.	Real	Imag.	Real	Imag.
C_{ℓ_δ}	0.0°	0.171	0.636	0.422	1.100	0.724	1.420	0.881	1.728
	0.42°	0.324	0.728	0.734	1.130	1.058	1.379	1.355	1.505
C_{ℓ_α}	0.0°	12.724	-3.409	11.001	-4.223	9.469	-4.825	8.642	-4.403
	0.42°	14.555	-6.480	11.303	-7.340	9.195	-7.055	7.524	-6.775
C_{m_δ}	0.0°	-0.008	-0.038	-0.015	-0.071	-0.022	-0.103	-0.029	-0.136
	0.42°	-0.043	-0.085	-0.092	-0.127	-0.137	-0.152	-0.180	-0.162
C_{m_α}	0.0°	-0.763	0.162	-0.706	0.150	-0.686	0.146	-0.680	0.145
	0.42°	-1.704	0.868	-1.272	0.924	-1.014	0.913	-0.811	0.901

Table 3 Aerodynamic Coefficients for MBB A-3 Airfoil at M = 0.765, and
$\alpha = 0.0^\circ$ and $\alpha = 0.75^\circ$ by Harmonic Analysis (UTRANS2) with 71x74 – Grid

	Angle, α	Reduced Frequency (k_c)									
		0.0		0.05		0.10		0.15		0.20	
		Real	Imag.	Real	Imag.	Real	Imag.	Real	Imag.	Real	Imag.
C_{ℓ_δ}	0.0°	0.0	0.0	0.089	0.521	0.260	0.900	0.523	1.185	0.772	1.288
	0.75°	0.0	0.0	0.119	0.557	0.279	0.906	0.539	1.172	0.772	1.277
C_{ℓ_α}	0.0°	11.221	0.0	10.141	-1.949	8.843	-2.801	7.667	-3.060	6.710	-2.970
	0.75°	11.388	0.0	10.171	-1.941	8.932	-2.818	7.757	-3.144	6.702	-3.180
C_{m_δ}	0.0°	0.0	0.0	0.003	-0.015	0.010	-0.031	0.017	-0.053	0.020	-0.076
	0.75°	0.0	0.0	-0.003	-0.035	-0.003	-0.060	-0.009	-0.090	-0.020	-0.113
C_{m_α}	0.0°	-0.311	0.0	-0.307	-0.074	-0.319	-0.148	-0.340	-0.212	-0.365	-0.265
	0.75°	-0.691	0.0	-0.640	0.006	-0.614	-0.023	-0.597	-0.056	-0.589	-0.073

Figure 9. Effect of Position of Mass Center on Flutter Speed for Three Plunge-to-Pitch Frequency Ratios for MBB A-3 Airfoil at M = 0.765 and α = 0.0° and 0.42° (by LTRAN2).

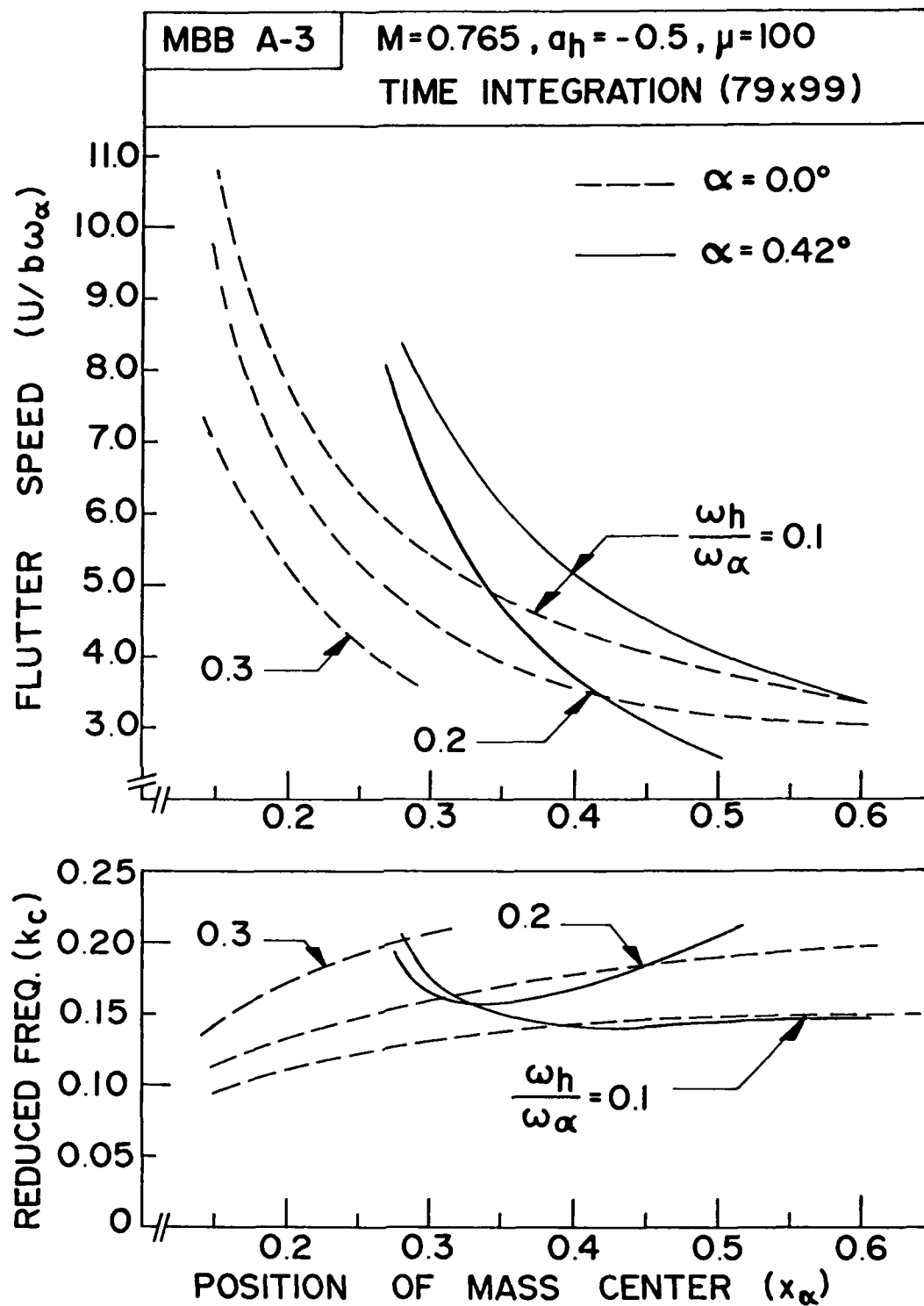Figure 10. Effect of Position of Mass Center on Flutter Speed for Four Plunge-to-Pitch Frequency Ratios for MBB A-3 Airfoil at M = 0.765 and α = 0.0° and 0.75° (by STRANS2/UTRANS2).

assumed as 100 and -0.5, respectively.

In both figures, equivalent sets of curves obtained for the case of zero angle of attack are also shown for comparison. Both sets of curves, with zero and nonzero angles of attack, show similar general trends.

It is seen that at the equivalent design angles of attack (0.42^O for LTRAN2 and 0.75^O for UTRANS2) the curves for flutter speed shift toward the right but still maintain the same trends. The shift is more pronounced in Figure 9 than Figure 10. Within the range of values assumed for all the parameters, it appears that the airfoil is in general more stable at the design conditions than at the zero-α conditions. However, in Figure 9 the flutter speed decreases with the increase in angle of attack for ω_h/ω_α = 0.2 and $x_\alpha > 0.42$.

Figures 9 and 10 show that it is difficult to obtain flutter speeds when the values of x_α are less than 0.3 and 0.2, respectively. In order to obtain meaningful flutter speeds in the following analysis for influences of camber and thickness distribution, the values for x_α were chosen as 0.35 and 0.25 for LTRAN2 and UTRANS2, respectively.

Figure 11 shows the curves for flutter speed and the corresponding reduced frequency versus the airfoil-air mass ratio obtained by LTRAN2 for two different values of frequency ratio. The values for x_α, a_h, and α were assumed as 0.35, -0.5, and 0.42^O, respectively. In the same figure an equivalent set of curves obtained for zero angle of attack is also shown for comparison. Similar sets of curves obtained by UTRANS2 for x_α = 0.25, a_h = -0.5, and α = 0.75^O are given in Figure 12.

In both figures, the two sets of curves, one with zero angle of attack and one with the equivalent design angles of attack, show a similar trend.

45

Figure 11. Effect of Airfoil-Air Mass Ratio on Flutter Speed for Three Plunge-to-Pitch Frequency Ratios for MBB A-3 Airfoil at M = 0.765 and α = 0.0[o] and 0.42[o] (by LTRAN2).

Figure 12. Effect of Airfoil-Air Mass Ratio on Flutter Speed for Three Plunge-to-Pitch Frequency Ratios for MBB A-3 Airfoil at M = 0.765 and $\alpha = 0.0°$ and $0.75°$ (by STRANS2/UTRANS2).
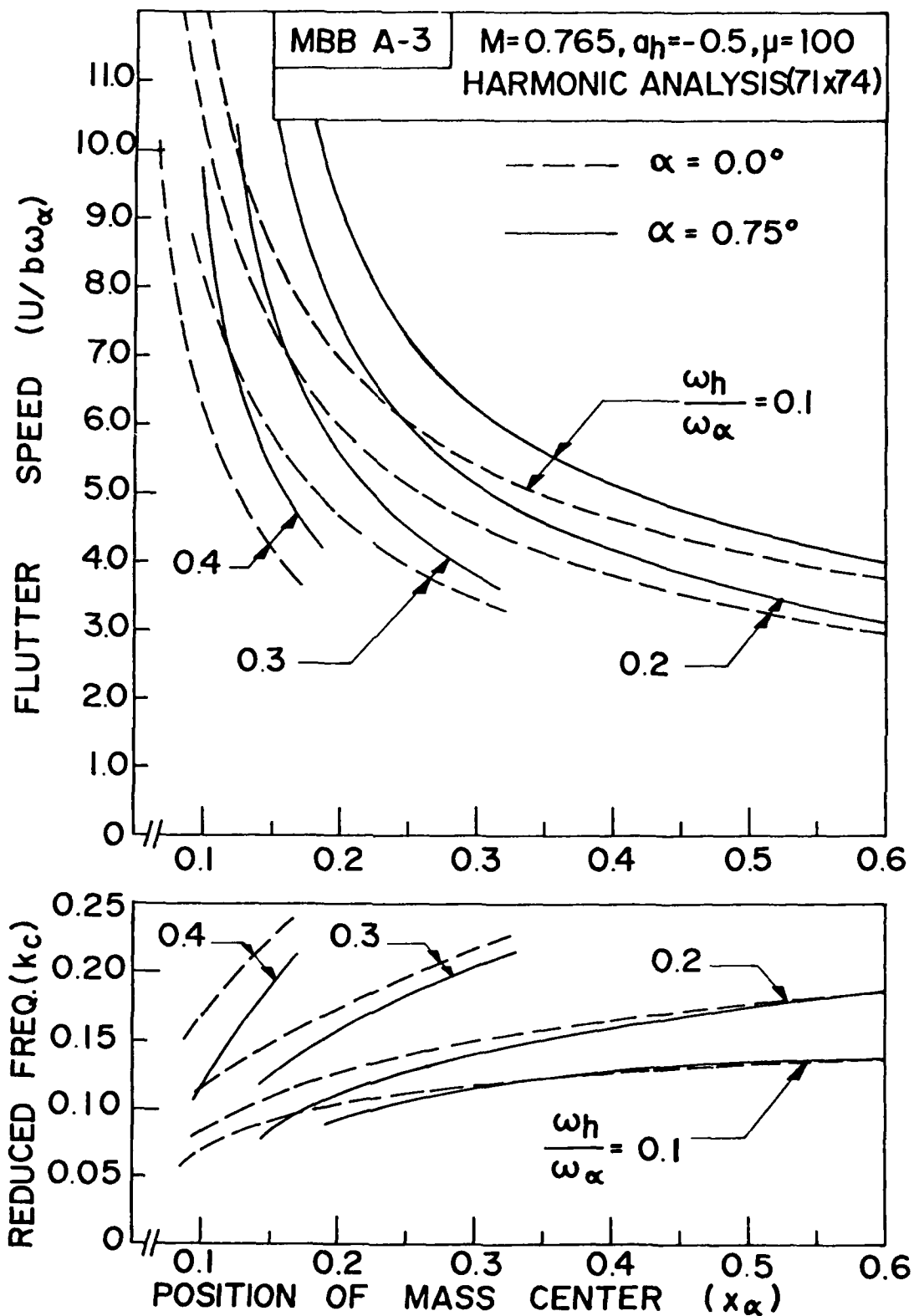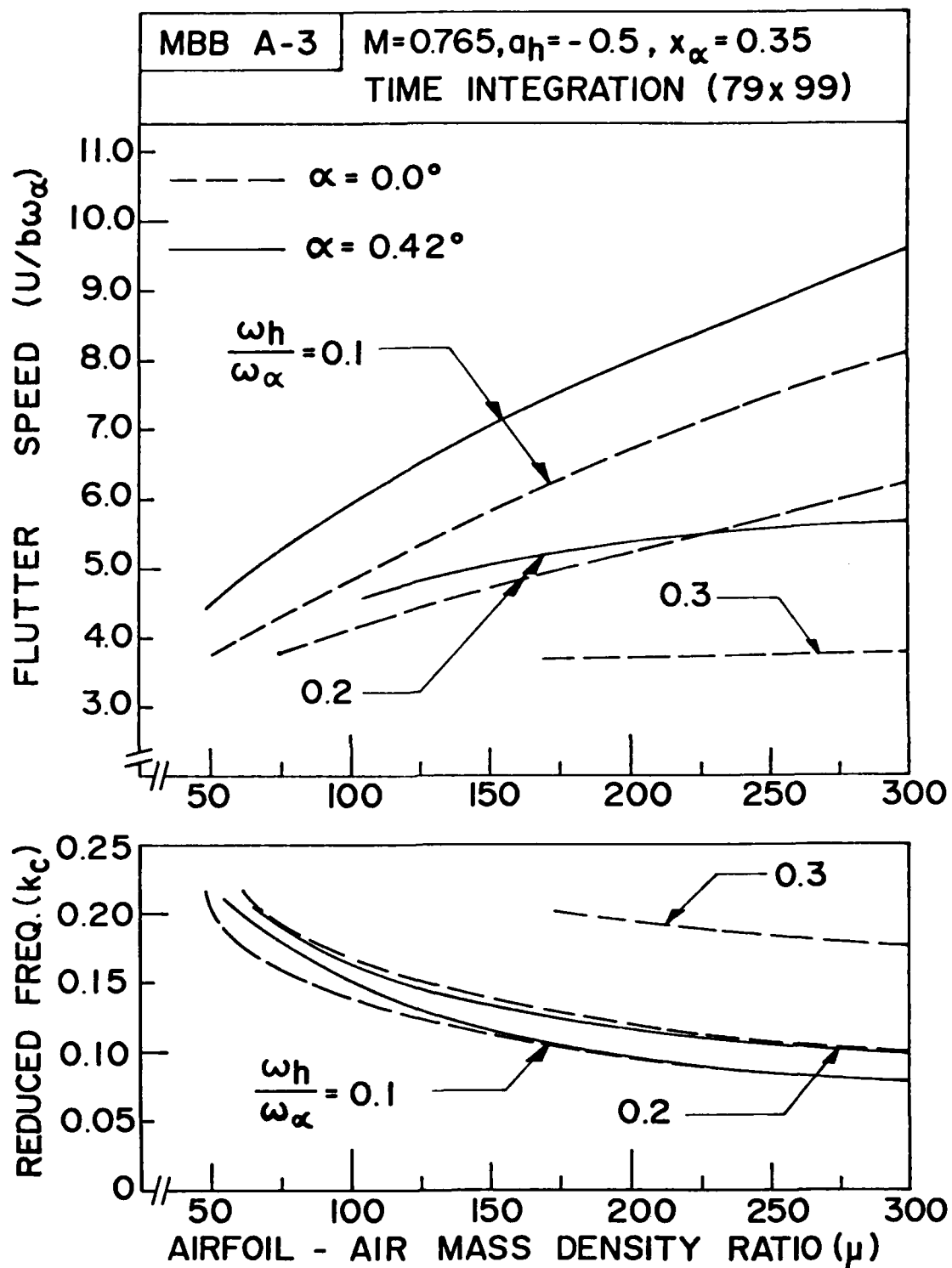
In both figures, the curves for flutter speed shift upward in the case of equivalent design angles of attack with the exception in Figure 11 for $\omega_h/\omega_\alpha = 0.2$. It appears that within the range of values assumed for most of the parameters, the airfoil is more stable at the design angles of attack than at the zero angle of attack. However, in Figure 11 the flutter speed decreases with the increase in angle of attack for $\omega_h/\omega_\alpha = 0.2$ and $\mu > 250$.

Figure 13 shows the curves for flutter speed and the corresponding reduced frequency versus the position of elastic axis obtained by LTRAN2 for three values of frequency ratio. These curves were obtained by fixing the mass center at 42.5%-chord and assuming the values for μ and α equal to 100 and 0.42^0, respectively. A corresponding set of curves obtained for the case of zero angle of attack is also shown in the same figure for comparison.

A similar analysis was carried out by using UTRANS2. This was done by fixing the mass center at 3/8-chord and assuming the values for μ and α equal to 100 and 0.75^0, respectively. The results are shown in Figure 14. In the same figure, a corresponding set of results obtained for $\alpha = 0^0$ is also shown for comparison.

In both figures the behavior of the curves for the case of equivalent design angles of attack is similar to that for the case of zero angle of attack. Furthermore, the trends obtained by the two separate computational methods are similar.

Again, both figures show that the flutter curves shift upward in the case of equivalent design angles of attack.

In summary, it may be concluded that, within the range of values assumed for the aeroelastic parameters, the MBB A-3 supercritical aeroelastic system is, in general, more stable at the equivalent design angles of attack than at
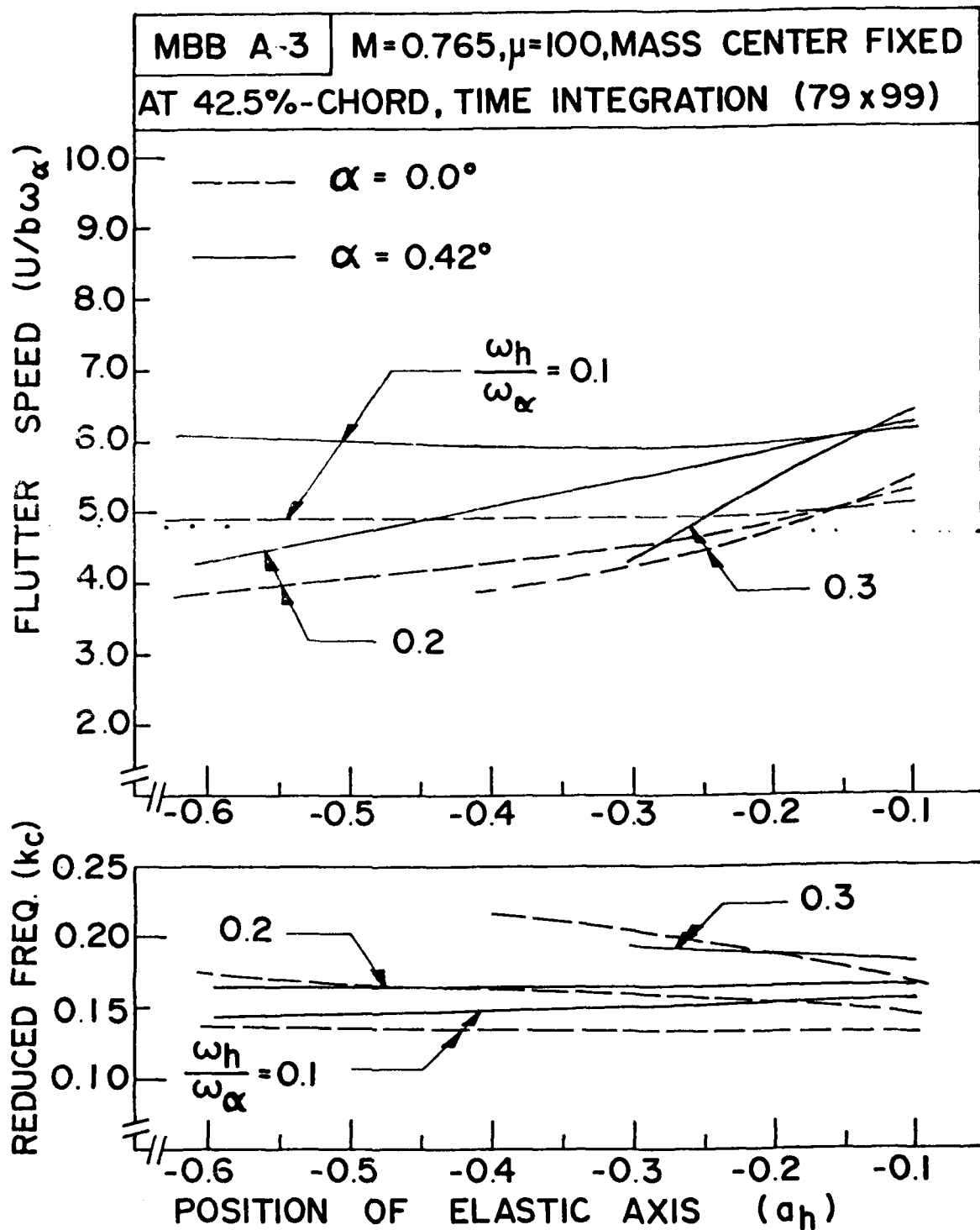
Figure 13. Effect of Position of Elastic Axis on Flutter Speed for Three Plunge-to-Pitch Frequency Ratios for MBB A-3 Airfoil at M = 0.765 and α = 0.0 and 0.42° (by LTRAN2).

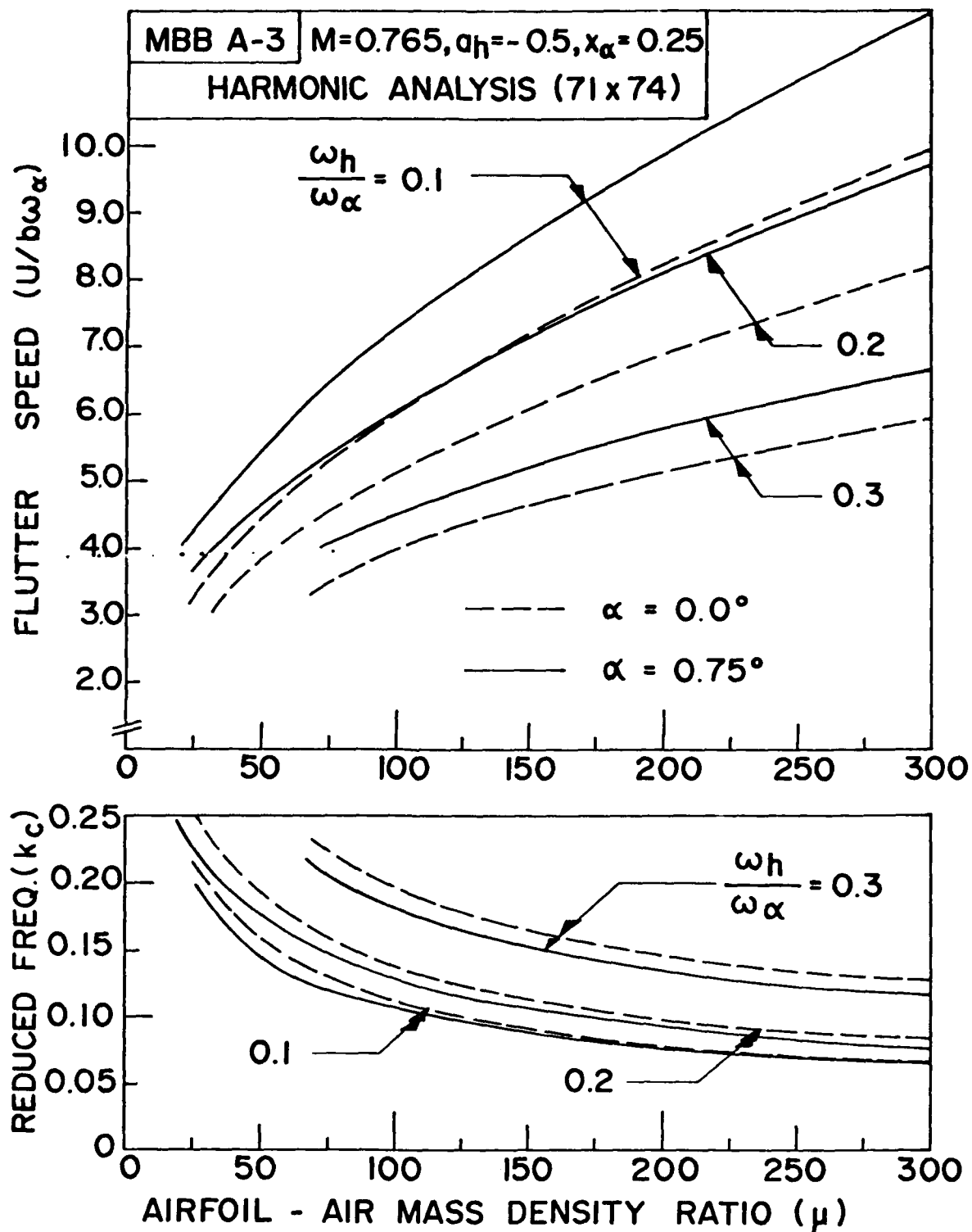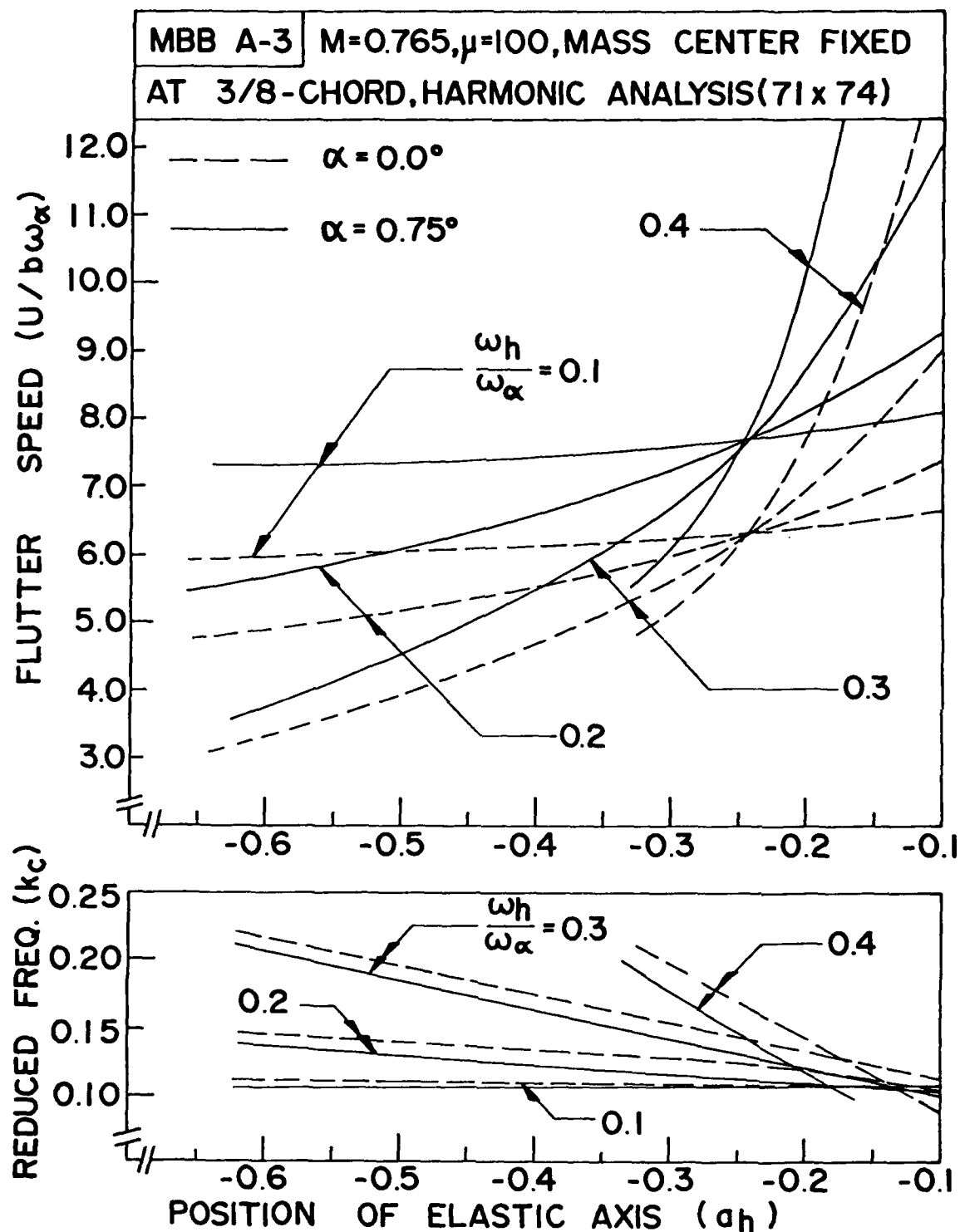Figure 14. Effect of Position of Elastic Axis on Flutter Speed for Four Plunge-to-Pitch Frequency Ratios for MBB A-3 Airfoil at M = 0.765 and $\alpha = 0.0^o$ and 0.75^o (by STRANS2/UTRANS2).

50

zero angle of attack.

5.4 Flutter Analysis of a MBB A-3 Airfoil without Camber

The MBB A-3 supercritical airfoil was designed with a camber. The camber influences the aerodynamic characteristics and in turn the aeroelastic behavior of the airfoil. It is of interest to study such influences by considering an airfoil obtained by removing the camber from the MBB A-3 supercritical airfoil and comparing the results with those obtained for the original airfoil with camber.

The profile for such a non-cambered version of the MBB A-3 airfoil is given in Section 5.1. The study of this airfoil was conducted for the design Mach number $M_\infty = 0.765$ and equivalent design angles of attack 0.42^O and 0.75^O for LTRAN2 and UTRANS2, respectively.

5.4.1 Steady Pressure Curves

Figure 15 shows the upper and lower surface pressure curves obtained for the MBB A-3 airfoil without camber by LTRAN2 at $M_\infty = 0.765$ and $\alpha = 0.42^O$. There is no shock in this case. The equivalent pressure curves obtained for the original MBB A-3 airfoil are also shown in the same figure. There is a fairly strong shock on the upper surface of the MBB A-3 airfoil.

Figure 16 shows the upper and lower surface pressure curves obtained for the MBB A-3 airfoil without camber by STRANS2 at $M_\infty = 0.765$ and $\alpha = 0.75^O$. Again, there is no shock in this case. The equivalent pressure curves for the original MBB A-3 airfoil are also shown. A fairly strong shock is seen.

5.4.2 Unsteady Aerodynamic Coefficients

Table 4 shows two sets of unsteady aerodynamic coefficients for the MBB A-3 airfoil, with and without camber, at $M_\infty = 0.765$ and $\alpha = 0.42^O$ obtained by the

51
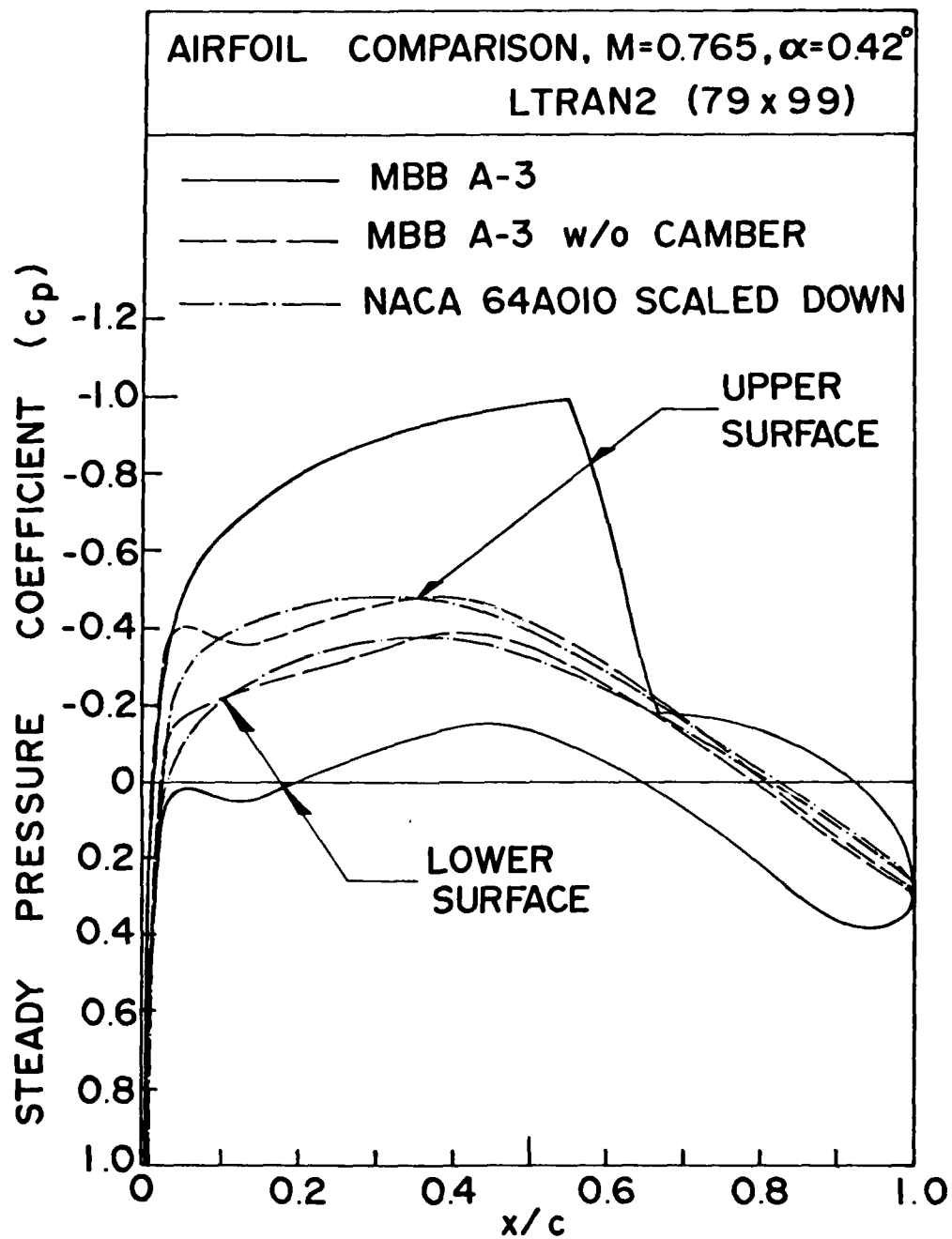
Figure 15. Distribution of Steady Pressure Coefficients for Airfoil Comparison at M = 0.765 and $\alpha = 0.42^\circ$ (by LTRAN2).
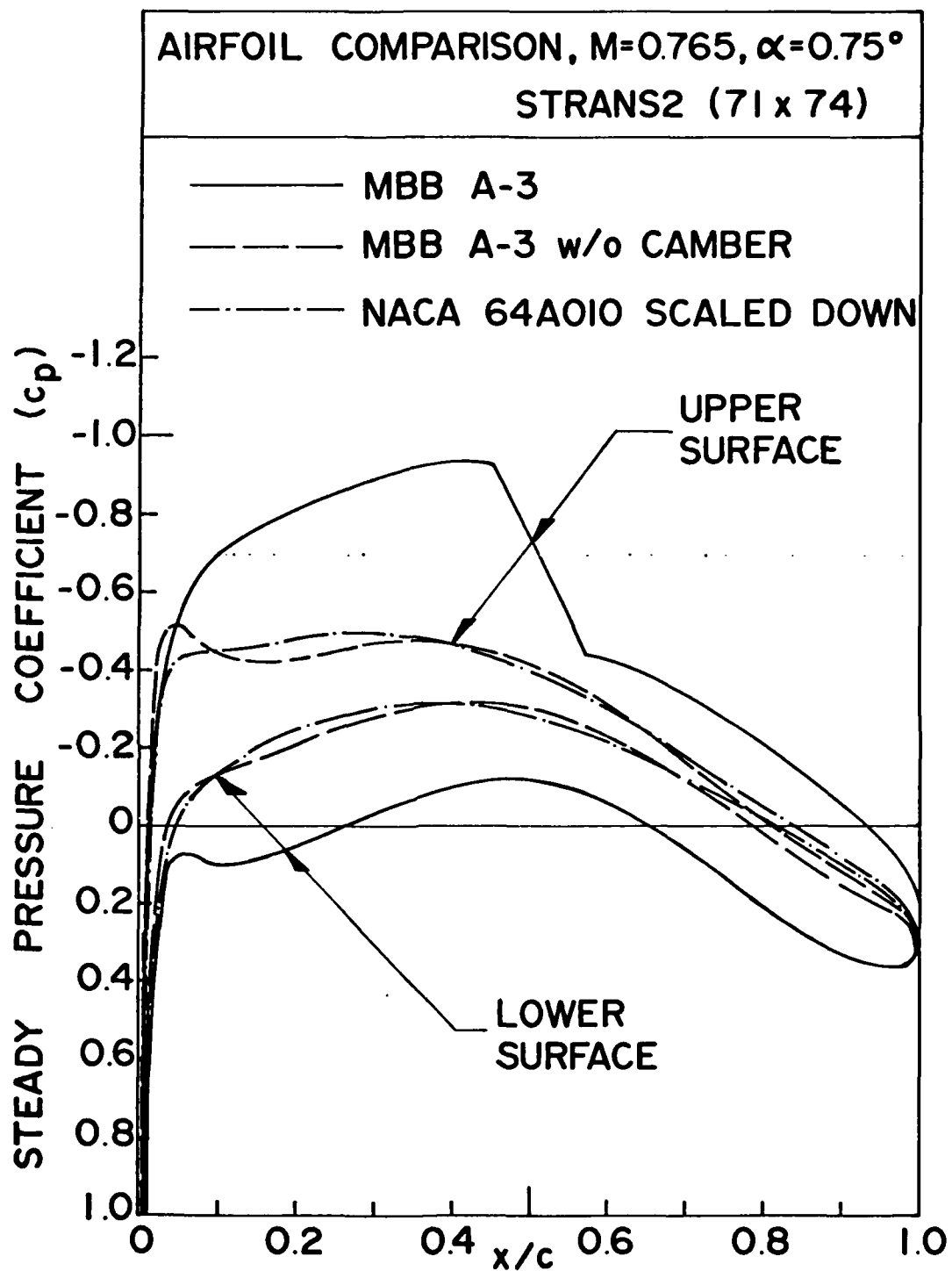
Figure 16. Distribution of Steady Pressure Coefficients for Airfoil Comparison
at M = 0.765 and α = 0.75° (by STRANS2).

53

Table 4   Aerodynamic Coefficients for Airfoil Comparison at M = 0.765
and α = 0.42° by Time Integration (LTRAN2) with 79x99 – Grid.

| | Airfoil | Reduced Frequency (k_c) | | | | | | | |
| | | 0.05 | | 0.10 | | 0.15 | | 0.20 | |
		Real	Imag.	Real	Imag.	Real	Imag.	Real	Imag.
C_{ℓ_δ}	1	0.324	0.728	0.734	1.130	1.058	1.379	1.355	1.505
	2	0.096	0.519	0.289	0.977	0.489	1.273	0.731	1.534
	3	0.097	0.521	0.279	0.940	0.516	1.343	0.825	1.731
C_{ℓ_α}	1	14.555	-6.480	11.303	-7.340	9.195	-7.055	7.524	-6.775
	2	10.385	-1.925	9.766	-2.893	8.489	-3.259	7.668	-3.657
	3	10.420	-1.931	9.403	-2.785	8.954	-3.437	8.653	-4.127
C_{m_δ}	1	-0.043	-0.085	-0.092	-0.127	-0.137	-0.152	-0.180	-0.162
	2	0.003	-0.005	0.008	-0.013	0.015	-0.024	0.024	-0.036
	3	0.003	-0.007	0.008	-0.014	0.015	-0.025	0.023	-0.040
C_{m_α}	1	-1.704	0.868	-1.272	0.924	-1.014	0.913	-0.811	0.901
	2	-0.105	-0.060	-0.129	-0.084	-0.158	-0.103	-0.182	-0.118
	3	-0.140	-0.067	-0.142	-0.082	-0.168	-0.103	-0.197	-0.114

Airfoil 1:   MBB A-3

Airfoil 2:   MBB A-3 without Camber

Airfoil 3:   NACA 64A010, Scaled Down to 8.9%
Thickness-to-Chord Ratio

54

time integration method (LTRAN2). Two similar sets of results obtained by the harmonic method (STRANS2) for $M_\infty = 0.765$ and $\alpha = 0.75^0$ are given in Table 5.

In both tables, it is seen that the magnitudes of both lift and moment coefficients are smaller in the case of no camber. Such reductions in magnitude are more pronounced in moment coefficients than in lift coefficients.

5.4.3 Flutter Results

Figures 17 and 18 show the effect of the position of mass center on the flutter results for the MBB A-3 airfoil without camber obtained by LTRAN2 and UTRANS2, respectively. Several values of frequency ratio ω_h/ω_α (0.1, 0.2, 0.3, and 0.4 in Figure 18, respectively) were considered. The values for μ and a_h were assumed as 100 and -0.5, respectively. In both figures, corresponding sets of curves for the original MBB A-3 airfoil are also shown for comparison.

Both figures show that the flutter speed increases as the mass center moves toward the elastic axis. Such increase becomes very sharp as the mass center gets close to the elastic axis. Both figures also show that the removal of the camber has an effect of shifting the curves toward the left. It appears that the camber has a stabilizing effect of increasing the flutter speed. Such effect is far more pronounced in the lower region of x_α.

Figures 19 and 20 show the curves for the flutter speed and the corresponding reduced frequency versus the airfoil-air mass ratio for several values of frequency ratio obtained by LTRAN2 and UTRANS2, respectively. The assumed values for x_α and a_h are given in the two figures.

Both figures show that flutter speed increases steadily with the increase of airfoil-air mass ratio. Removal of the camber shows an obvious destabilizing

Table 5 Aerodynamic Coefficients for Airfoil Comparison at M = 0.765
and α = 0.75° by Harmonic Analysis (UTRANS2) with 71x74 - Grid

| | Airfoil | Reduced Frequency (k_c) | | | | | | | | | |
| | | 0.0 | | 0.05 | | 0.10 | | 0.15 | | 0.20 | |
		Real	Imag.	Real	Imag.	Real	Imag.	Real	Imag.	Real	Imag.
C_{ℓ_δ}	1	0.0	0.0	0.119	0.557	0.279	0.906	0.539	1.172	0.772	1.277
	2	0.0	0.0	0.087	0.504	0.266	0.873	0.491	1.142	0.702	1.298
	3	0.0	0.0	0.076	0.493	0.265	0.870	0.492	1.141	0.705	1.295
C_{ℓ_α}	1	11.388	0.0	10.171	-1.941	8.932	-2.818	7.757	-3.144	6.702	-3.180
	2	10.760	0.0	9.796	-1.749	8.661	-2.479	7.660	-2.722	6.793	-2.734
	3	10.766	0.0	9.807	-1.767	8.660	-2.502	7.650	-2.744	6.777	-2.752
C_{m_δ}	1	0.0	0.0	-0.003	-0.035	-0.003	-0.060	-0.009	-0.090	-0.020	-0.113
	2	0.0	0.0	0.003	-0.009	0.011	-0.019	0.021	-0.034	0.030	-0.052
	3	0.0	0.0	0.003	-0.009	0.010	-0.021	0.019	-0.036	0.028	-0.053
C_{m_α}	1	-0.691	0.0	-0.640	0.006	-0.614	-0.023	-0.597	-0.056	-0.589	-0.073
	2	-0.166	0.0	-0.172	-0.090	-0.192	-0.172	-0.218	-0.241	-0.244	-0.297
	3	-0.187	0.0	-0.191	-0.084	-0.208	-0.162	-0.230	-0.230	-0.254	-0.285

Airfoil 1:   MBB A-3
Airfoil 2:   MBB A-3 without Camber
Airfoil 3:   NACA 64A010, Scaled Down to 8.9%
             Thickness-to-Chord Ratio

Figure 17. Effect of Position of Mass Center on Flutter Speed for Three Plunge-to-Pitch Frequency Ratios for Airfoil Comparison at M = 0.765 and α = 0.42° (by LTRAN2).

Figure 18. Effect of Position of Mass Center on Flutter Speed for Four Plunge-to-Pitch Frequency Ratios for Airfoil Comparison at M = 0.765 and α = 0.75° (by STRANS2/UTRANS2).

Figure 19. Effect of Airfoil-Air Mass Ratio on Flutter Speed for Three Plunge-to-Pitch Frequency Ratios for Airfoil Comparison at M = 0.765 and α = 0.42° (by LTRAN2).

59

Figure 20. Effect of Airfoil-Air Mass Ratio on Flutter Speed for Four Plunge-to-Pitch Frequency Ratios for Airfoil Comparison at M = 0.765 and α = 0.75° (by STRANS2/UTRANS2).

effect that reduces the flutter speed.

Figures 21 and 22 show the curves for the flutter speed and the corresponding reduced frequency versus the position of elastic axis for various values of plunge-to-pitch frequency ratio obtained by LTRAN2 and UTRANS2, respectively. The curves were obtained by fixing the mass center at 42.5% and 37.5%-chord in Figures 21 and 22, respectively. The μ value was chosen as 100 for both figures.

Both figures show that the flutter speed increases as the elastic axis moves toward the mid-chord position. Such increase is less pronounced for smaller values of frequency ratio and it becomes unnoticeable as $\omega_h/\omega_\alpha = 0.1$. As the mass center and elastic axis coincide, the flutter speed becomes independent of frequency ratio and all the flutter curves intersect at one point. Such phenomenon has been observed and explained in Reference 20.

Both figures show that as the camber is removed, flutter speed drops quite substantially.

In summary, it may be concluded from the results of Figures 17-22 that the camber of the MBB A-3 supercritical airfoil appears to have an important stabilizing effect that generally increases the flutter speed of the airfoil at the design operating conditions.

5.5 Flutter Analysis of a NACA 64A010 Airfoil Scaled-Down to 8.9%
     Maximum Thickness - Chord Ratio

An airfoil obtained by scaling down the thickness of the NACA 64A010 airfoil configuration by 11% is investigated. For simplicity, this model will be termed as "scaled-down conventional model." As shown in Figure 2, this model has a configuration very much alike the MBB A-3 airfoil without camber. Both models have the same maximum thickness-chord ratio. A study of the airfoil profile equations shows that the latter has a slightly blunter nose than the former.
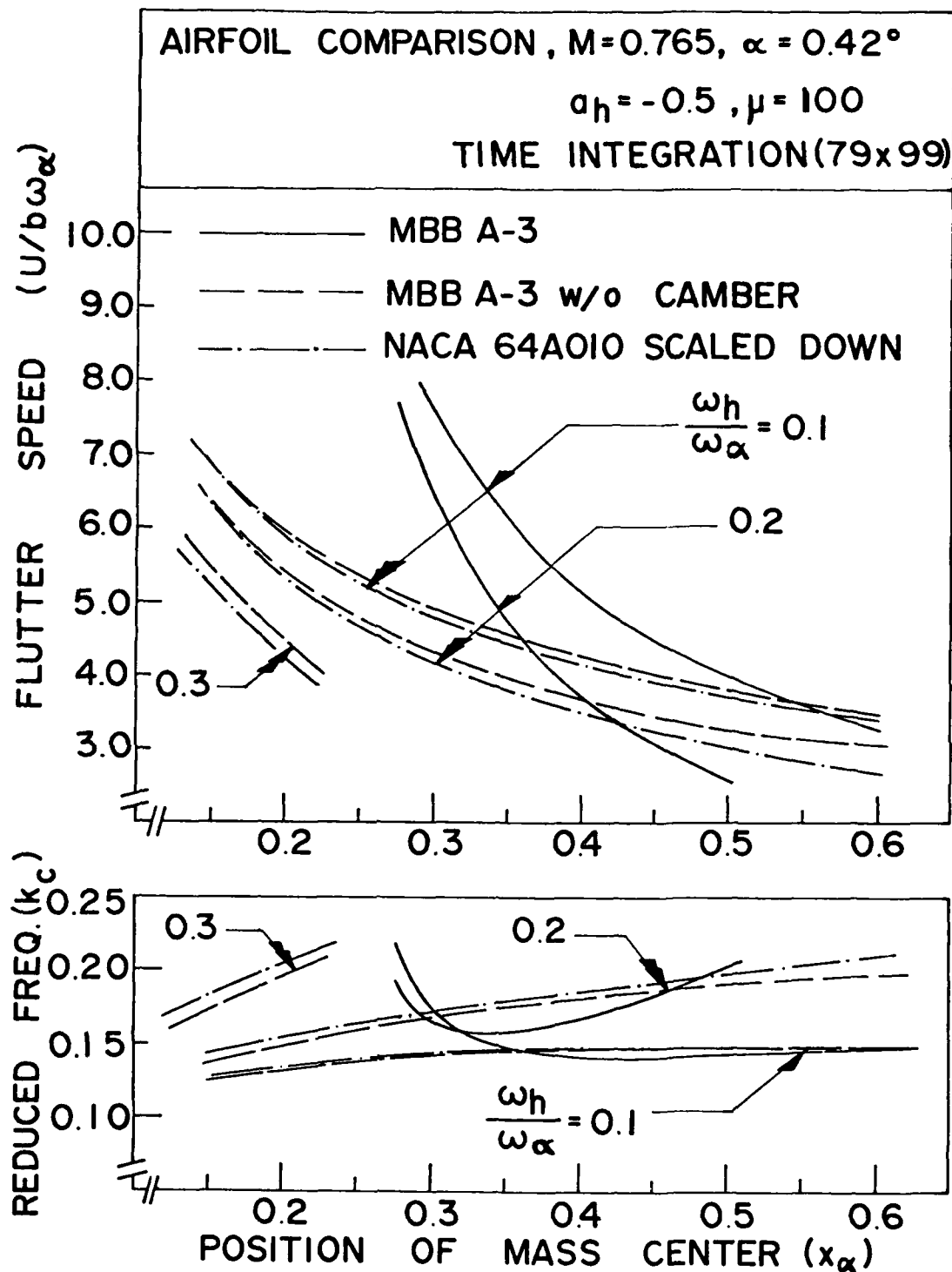
61

Figure 21.   Effect of Position of Elastic Axis on Flutter Speed for Three Plunge-
to-Pitch Frequency Ratios for Airfoil Comparison at M = 0.765 and
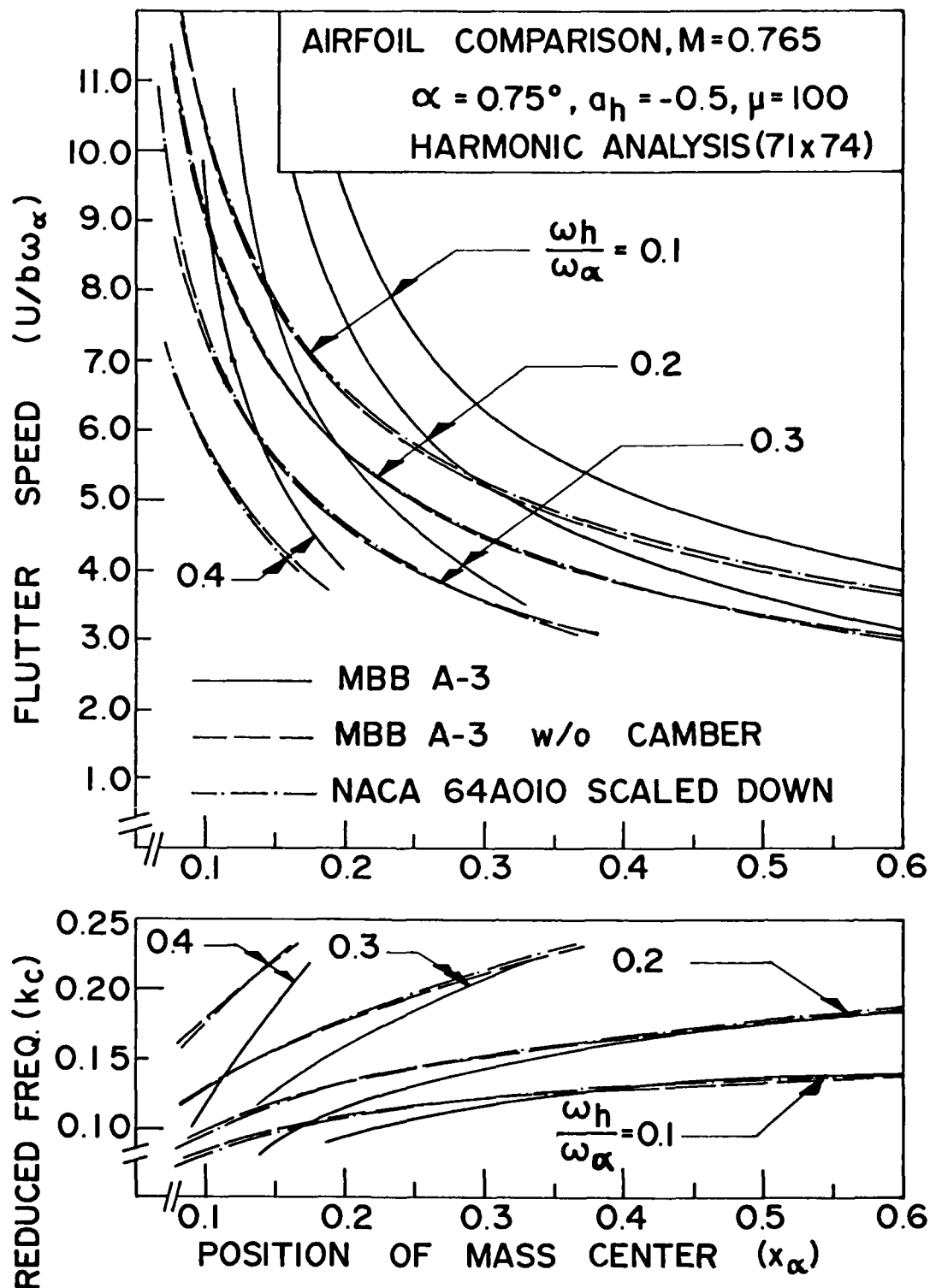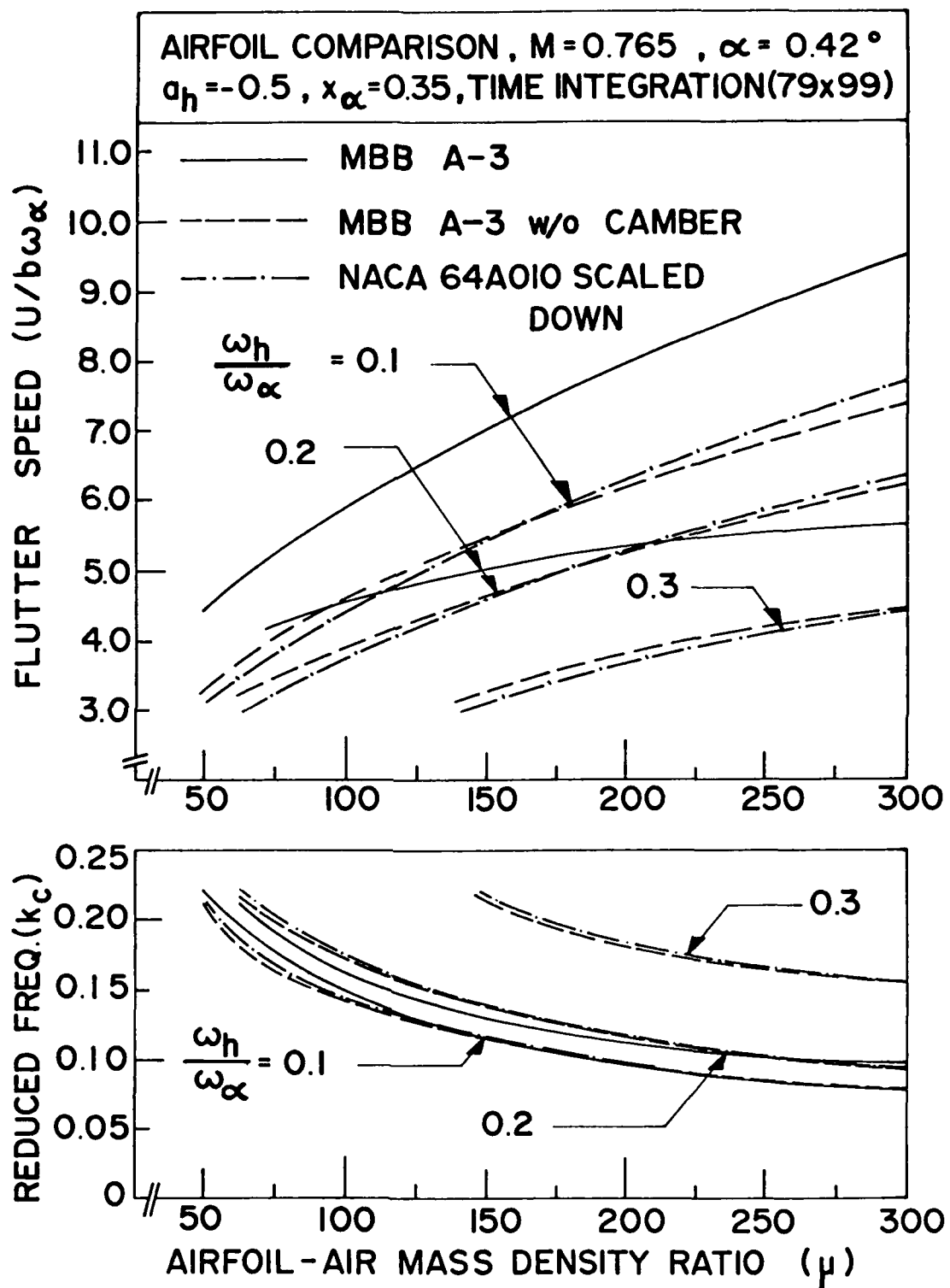$\alpha = 0.42^o$ (by LTRAN2).

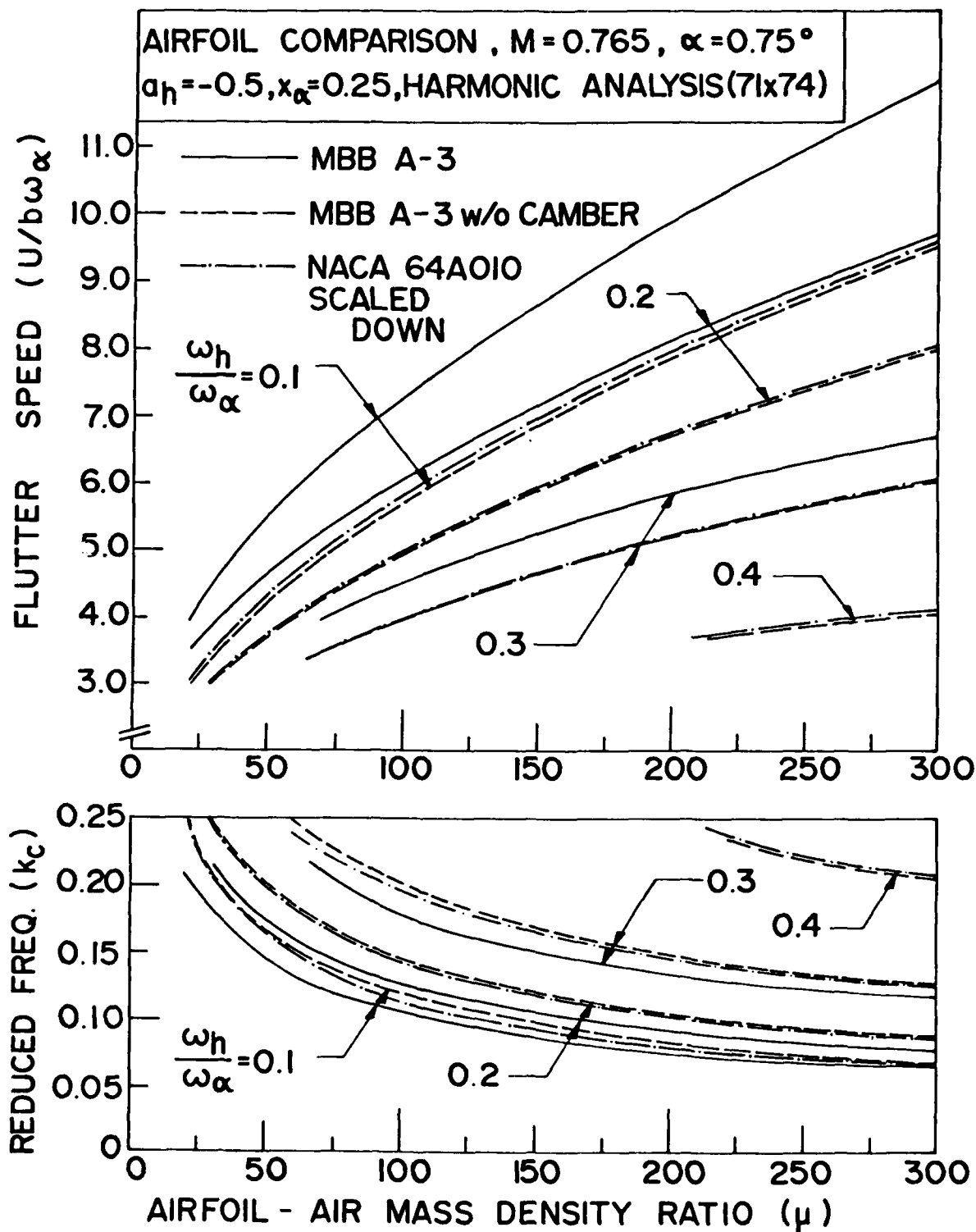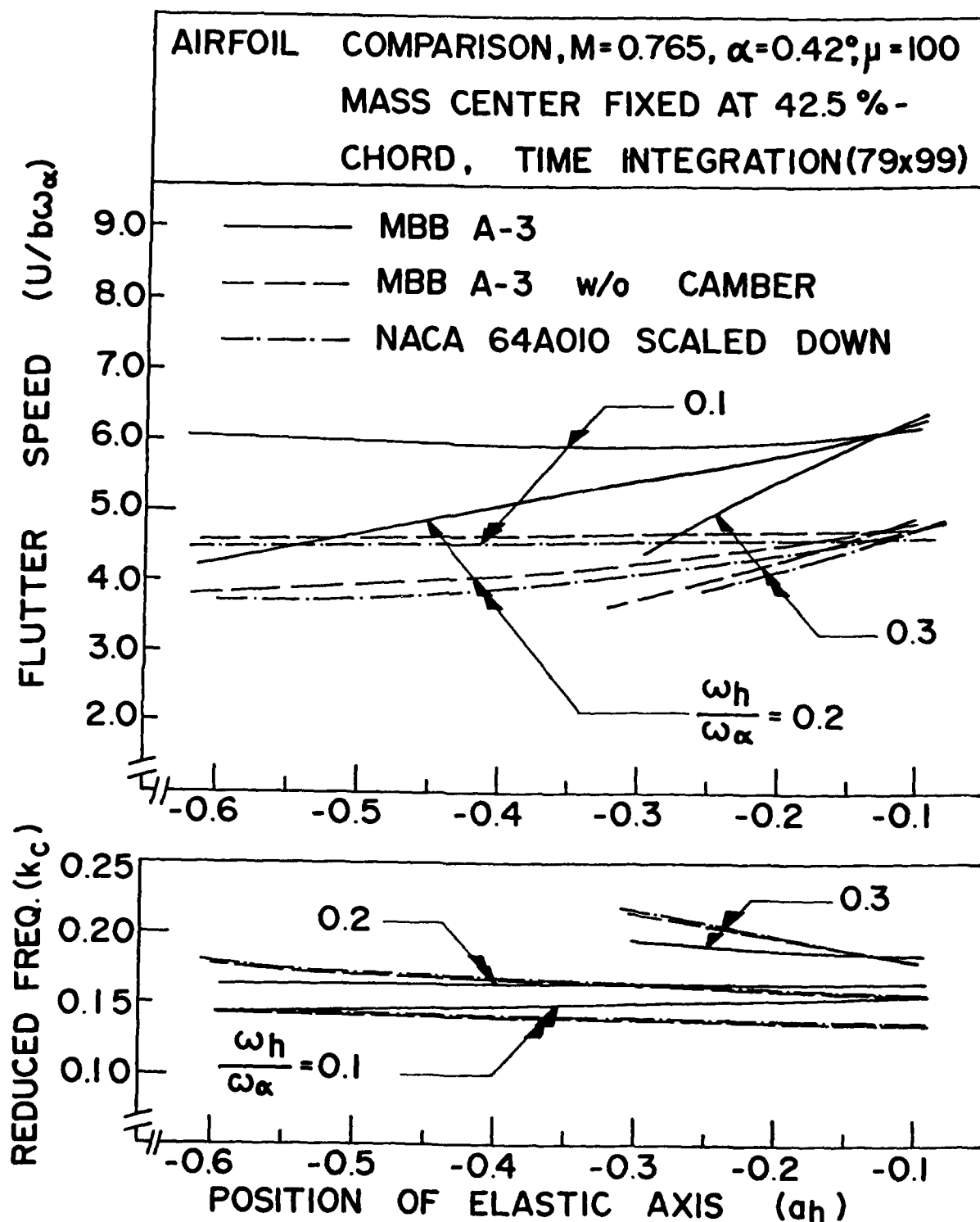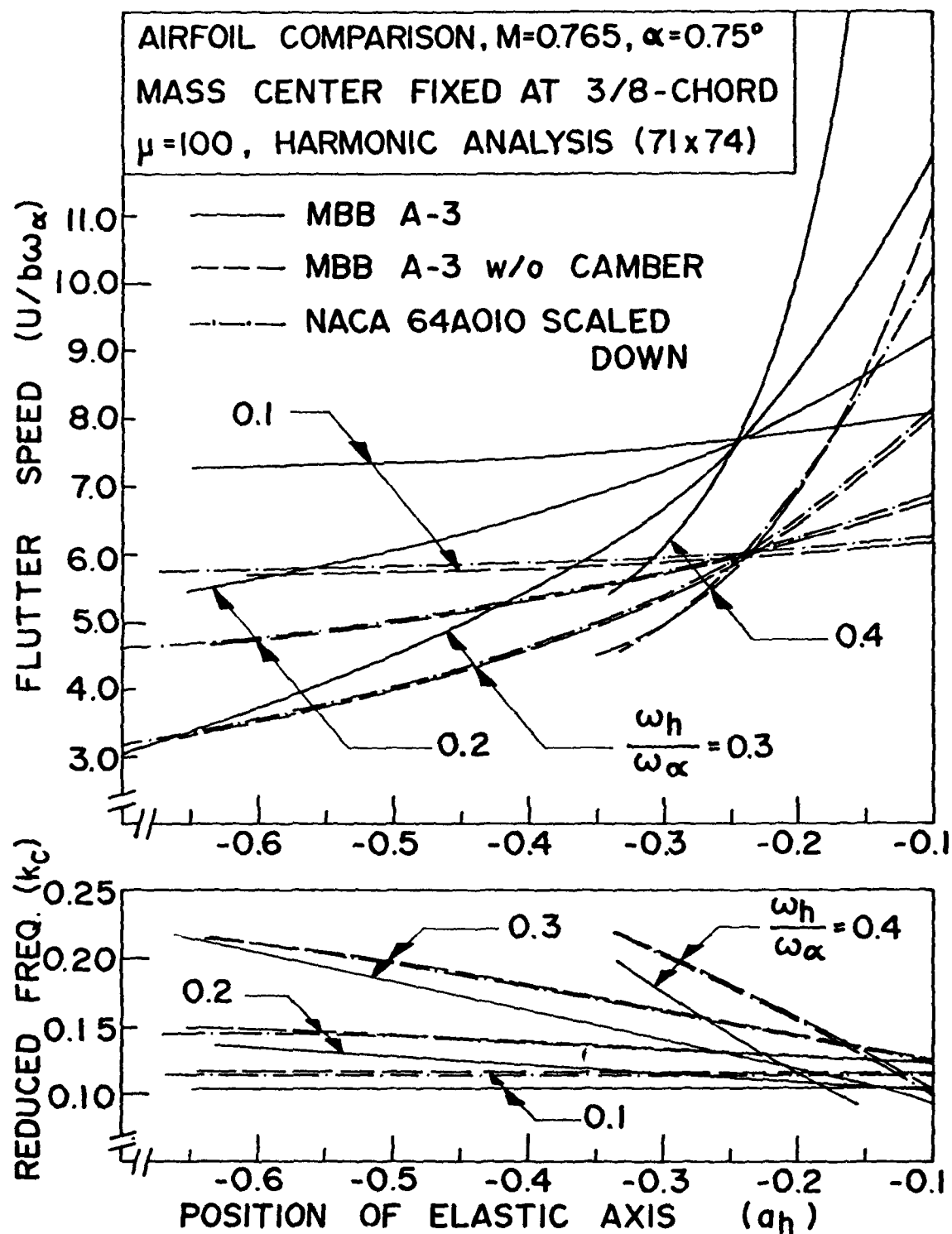Figure 22. Effect of Position of Elastic Axis on Flutter Speed for Four Plunge-to-Pitch Frequency Ratios for Airfoil Comparison at M = 0.765 and $\alpha = 0.75^{\circ}$ (by STRANS2/UTRANS2).

63

The purpose of this section is to study and compare the aerodynamic and flutter characteristics between the scaled-down conventional model with "conventional" variation of thickness and the MBB A-3 model without camber but with "supercritical" variation of thickness.

For clarity of presentation and simplicity of comparison, the aerodynamic and flutter results for the scaled-down conventional model are plotted together with those obtained for the MBB A-3 airfoil and MBB A-3 airfoil without camber (Figures 15-22). This study was carried out for $M_\infty = 0.765$ and $\alpha = 0.42^\circ$ and 0.75° for LTRAN2 and STRANS2/UTRANS2, respectively.

5.5.1 Steady Pressure Curves

The curves for steady pressure distribution obtained by the programs LTRAN2 and STRANS2 for the scaled-down conventional model are shown in Figures 15 and 16, respectively, so that they can be compared with those for the MBB A-3 airfoil without camber.

Both figures show that the steady pressure distribution curves are very similar between the two models. However, the upper pressure curves for the MBB A-3 airfoil without camber present a small bump near the leading edge, probably due to the blunter nose.

5.5.2 Unsteady Aerodynamic Coefficients

The results for the unsteady aerodynamic coefficents for the scaled-down conventional model pitching about the 1/4-chord axis obtained by LTRAN2 and UTRANS2 are given in Tables 4 and 5, respectively, so that they can be compared with those obtained for the MBB A-3 airfoil without camber.

Due to the close resemblance in configuration between the two models, both tables show that the unsteady aerodynamic coefficients are almost the

same between the two models.

5.5.3 Flutter Results

The results of flutter analysis for the MBB A-3 airfoil with and without camber have been presented in Figures 17-22 for various aeroelastic parameters. The corresponding results obtained for the scaled-down conventional model are also shown in Figures 17-22 for comparison.

Because the scaled-down conventional model and the MBB A-3 airfoil without camber have very similar configurations and nearly the same unsteady aerodynamic coefficients, the flutter curves obtained for the two models are in very close agreement in all figures (17 to 22). Thus it may be concluded that the supercritical thickness variation of the MBB A-3 airfoil without camber does not appear to affect the aeroelastic characteristics as compared to the conventional thickness variation.

5.6 Flutter Analysis of the MBB A-3 Supercritical Airfoil at $\alpha = 0^0$ with Various Mach Numbers

Studies conducted earlier for several airfoils (see, for example, References 16, 17, and 20) have shown that the curve for flutter speed versus Mach number exhibits a dip in the transonic regime. In this section, such transonic dip phenomenon is investigated for the MBB A-3 supercritical airfoil oscillating at zero mean angle of attack. Both programs LTRAN2 and STRANS2/UTRANS2 were used and the results were compared. The Mach numbers considered were 0.7, 0.72, 0.74, 0.765, and 0.78, respectively.

5.6.1 Steady Pressure Curves

Figures 23 and 24 show the pressure distribution curves on the upper and lower surfaces for the MBB A-3 supercritical airfoil at five different Mach
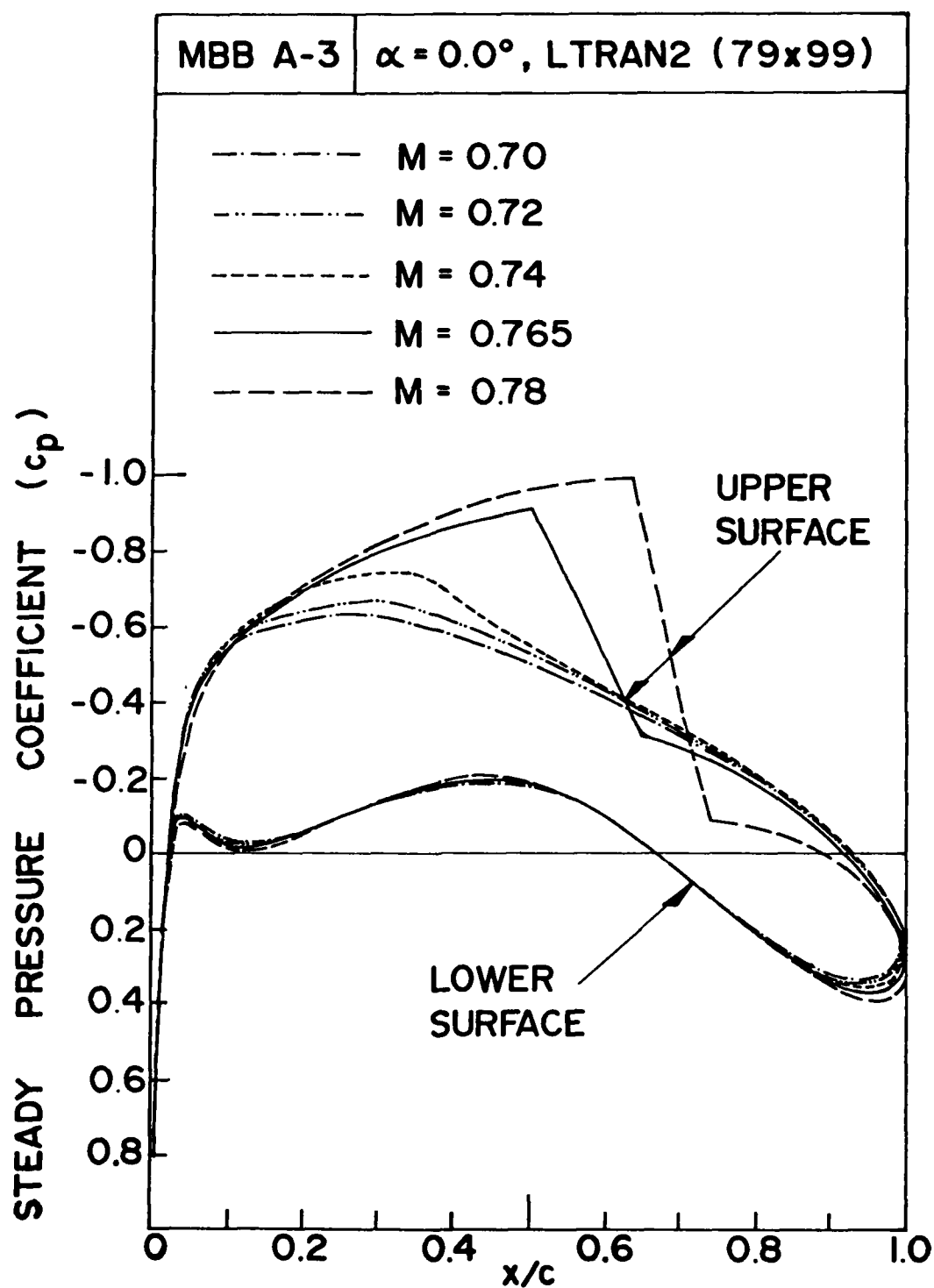
Figure 23. Distribution of Steady Pressure Coefficients for MBB A-3 Airfoil at Various Mach Numbers and $\alpha = 0.0^{\circ}$ (by LTRAN2).
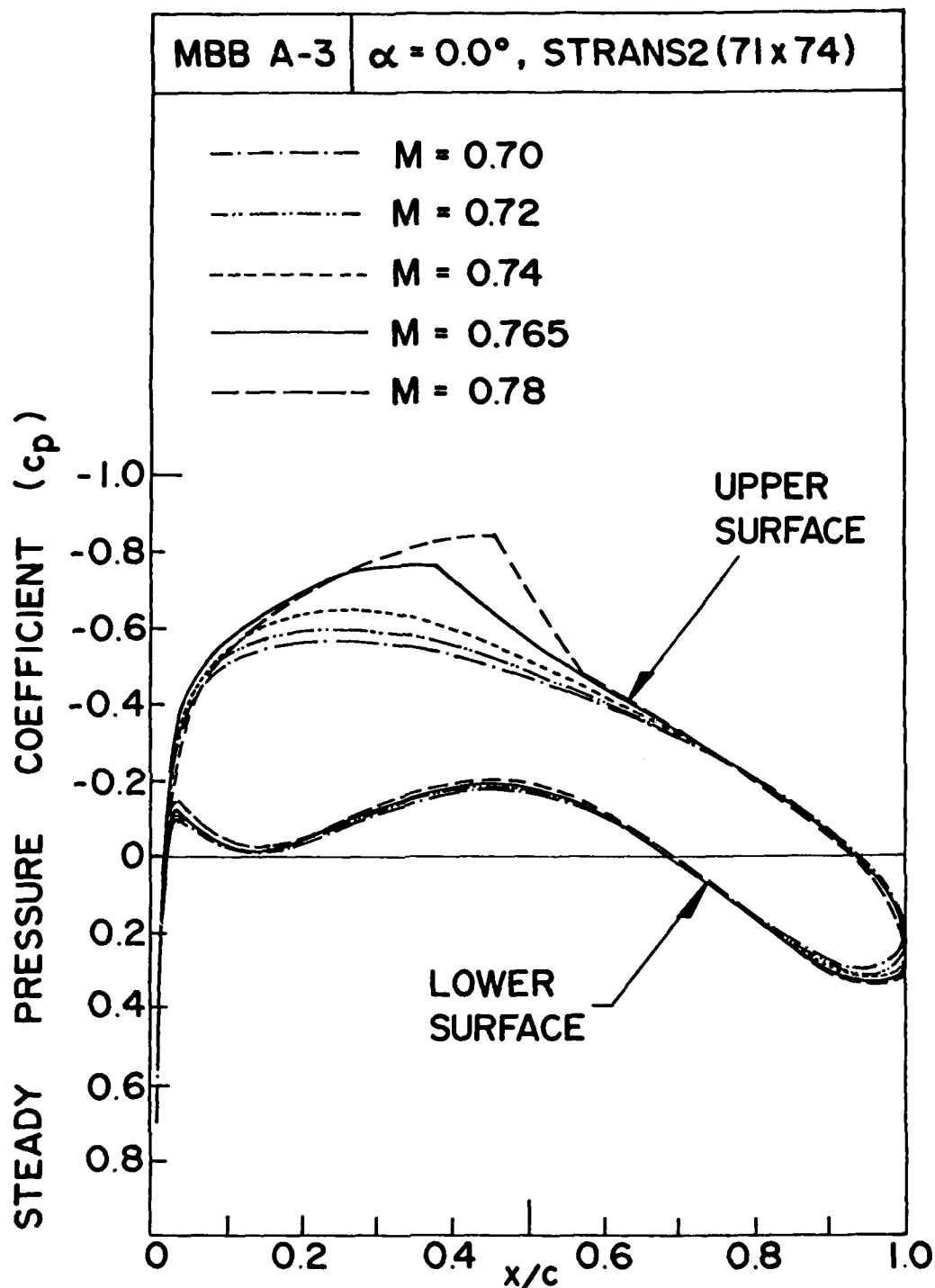
Figure 24. Distribution of Steady Pressure Coefficients for MBB A-3 Airfoil at Various Mach Numbers and $\alpha = 0.0^{0}$ (by STRANS2)

numbers (0.70, 0.72, 0.74, 0.765, and 0.78) obtained by LTRAN2 and STRANS2, respectively.

In both figures, the pressure curves on the upper surface grow rapidly with the increase in Mach number. On the other hand, the pressure curves on the lower surface change relatively much less with the increase in Mach number.

In both figures, the shocks start to develop at Mach numbers between 0.74 and 0.765. The shocks obtained by LTRAN2 as shown in Figure 23 are stronger thar these obtained by STRANS2 as shown in Figure 24. The shocks in Figure 23 are closer to the trailing edge than those in Figure 24. The discrepancies in the pressure curves between the two figures are most pronounced at $M_\infty = 0.78$. Such discrepancies result in differences between the unsteady aerodynamic coefficients obtained by the two programs.

From both figures it can be concluded that both the steady lift and moment coefficients increase with the increase in Mach number. The steady moment coefficients increase more rapidly than the steady lift coefficients.

5.6.2 Unsteady Aerodynamic Coefficients

Table 6 shows the unsteady aerodynamic coefficients obtained by using LTRAN2 for the MBB A-3 supercritical airfoil pitching about the quarterchord axis. The Mach numbers considered were 0.7, 0.72, 0.74, 0.765, and 0.78, res- pectively, and the reduced frequencies k_c considered were 0.05, 0.10, 0.15, and 0.2, respectively. Table 7 shows the corresponding results obtained by UTRANS2. The reduced frequencies considered were 0.0, 0.05, 0.10, 0.15, and 0.2, respectively.

The agreement between the two tables is better at lower Mach numbers. The discrepancies are largest at $M_\infty = 0.78$. As explained earlier, such discrepancies

Table 6 Aerodynamic Coefficients for MBB A-3 Airfoil for Various Mach Numbers at $\alpha = 0.0^{\circ}$ by Time Integration (LTRAN2) with 79x99 Grid

| | Mach Number | Reduced Frequency (k_c) | | | | | | | |
| | | 0.05 | | 0.10 | | 0.15 | | 0.20 | |
		Real	Imag.	Real	Imag.	Real	Imag.	Real	Imag.
C_{l_δ}	0.700	0.061	0.462	0.184	0.868	0.360	1.215	0.556	1.569
	0.720	0.077	0.483	0.215	0.897	0.404	1.244	0.592	1.543
	0.740	0.095	0.515	0.278	0.937	0.493	1.283	0.700	1.572
	0.765	0.171	0.636	0.422	1.100	0.724	1.420	0.881	1.728
	0.780	0.569	0.783	1.024	1.079	1.308	1.241	1.529	1.306
C_{l_α}	0.700	9.246	-1.217	8.677	-1.844	8.097	-2.398	7.845	-2.778
	0.720	9.652	-1.529	8.971	-2.154	8.296	-2.696	7.717	-2.962
	0.740	10.296	-1.908	9.374	-2.777	8.552	-3.283	7.862	-3.500
	0.765	12.724	-3.409	11.001	-4.223	9.469	-4.825	8.642	-4.403
	0.780	15.654	-11.373	10.794	-10.243	8.276	-8.721	6.531	-7.647
C_{m_δ}	0.700	0.002	-0.003	0.006	-0.007	0.011	-0.012	0.018	-0.020
	0.720	0.003	-0.003	0.007	-0.008	0.014	-0.015	0.020	-0.025
	0.740	0.003	-0.005	0.008	-0.012	0.016	-0.022	0.024	-0.036
	0.765	-0.008	-0.038	-0.015	-0.071	-0.022	-0.103	-0.029	-0.136
	0.780	-0.117	-0.144	-0.212	-0.172	-0.274	-0.178	-0.321	-0.164
C_{m_α}	0.700	-0.057	-0.037	-0.069	-0.056	-0.083	-0.075	-0.099	-0.089
	0.720	-0.062	-0.050	-0.077	-0.074	-0.101	-0.091	-0.126	-0.102
	0.740	-0.091	-0.059	-0.115	-0.083	-0.146	-0.106	-0.182	-0.118
	0.765	-0.763	0.162	-0.706	0.150	-0.686	0.146	-0.630	0.145
	0.780	-2.879	2.331	-1.719	2.122	-1.185	1.824	-0.818	1.606

Table 7 Aerodynamic Coefficients for MBD A-3 Airfoil for Various Mach Numbers at $\alpha = 0.0^{o}$ by Harmonic Analysis (UTRANS2) with 71x74 -Grid

	Mach Number	Reduced Frequency (k_c)									
		0.0		0.05		0.10		0.15		0.20	
		Real	Imag.	Real	Imag.	Real	Imag.	Real	Imag.	Real	Imag.
C_{l_δ}	0.700	0.0	0.0	0.045	0.448	0.170	0.793	0.337	1.093	0.517	1.323
	0.720	0.0	0.0	0.060	0.456	0.195	0.818	0.379	1.116	0.579	1.323
	0.740	0.0	0.0	0.068	0.475	0.229	0.850	0.437	1.138	0.648	1.327
	0.765	0.0	0.0	0.089	0.521	0.260	0.900	0.523	1.185	0.772	1.288
	0.780	0.0	0.0	0.102	0.515	0.311	0.877	0.557	1.105	0.746	1.204
C_{l_α}	0.700	9.205	0.0	9.096	-0.560	7.971	-1.598	7.334	-1.869	6.749	-1.964
	0.720	9.598	0.0	8.961	-1.230	8.185	-1.803	7.469	-2.118	6.802	-2.202
	0.740	10.233	0.0	9.400	-1.450	8.487	-2.130	7.631	-2.441	6.864	-2.499
	0.765	11.221	0.0	10.141	-1.949	8.843	-2.801	7.667	-3.060	6.710	-2.970
	0.780	11.244	0.0	9.975	-2.047	8.664	-2.824	7.522	-3.068	6.514	-3.058
C_{m_δ}	0.700	0.0	0.0	0.002	-0.008	0.008	-0.017	0.016	-0.029	0.026	-0.042
	0.720	0.0	0.0	0.002	-0.009	0.009	-0.018	0.018	-0.030	0.028	-0.045
	0.740	0.0	0.0	0.003	-0.009	0.010	-0.019	0.020	-0.033	0.030	-0.050
	0.765	0.0	0.0	0.003	-0.015	0.010	-0.031	0.017	-0.053	0.020	-0.076
	0.780	0.0	0.0	-0.003	-0.034	-0.008	-0.063	-0.015	-0.090	-0.027	-0.112
C_{m_α}	0.700	-0.168	0.0	-0.171	-0.082	-0.175	-0.135	-0.188	-0.197	-0.202	-0.253
	0.720	-0.170	0.0	-0.172	-0.074	-0.182	-0.145	-0.199	-0.209	-0.216	-0.266
	0.740	-0.170	0.0	-0.173	-0.083	-0.189	-0.161	-0.211	-0.229	-0.235	-0.288
	0.765	-0.311	0.0	-0.307	-0.074	-0.319	-0.148	-0.340	-0.212	-0.365	-0.265
	0.780	-0.720	0.0	-0.663	0.025	-0.625	-0.002	-0.601	-0.037	-0.587	-0.054

may be attributed to: (1) the basic difference in steady pressure curves; (2) different assumptions; and (3) different finite difference schemes.

The magnitudes of both the lift and moment coefficients obtained by both methods increase with the increase in Mach number. The rate of increase for the moment coefficients is higher than that for the lift coefficients. The rate of increase of both lift and moment coefficients shown in Table 6 is higher than that shown in Table 7. This may be due to the fact that the shock obtained by LTRAN2 grows faster than the shock obtained by UTRANS2.

5.6.3 Flutter Results

Based on the unsteady aerodynamic coefficients obtained in Tables 6 and 7 for the five different Mach numbers, flutter anlaysis was performed for the MBB A-3 supercritical airfoil. The emphasis was to investigate the effect of Mach number on flutter speed for various values of aeroelastic parameters.

Figure 25 shows two sets of curves for flutter speed and the corresponding reduced frequency versus Mach number for four different values of the parameter for the position of mass center (x_α = 0.3, 0.4, 0.5, and 0.6, respectively). One set is associated with the time integration method and the other set is associated with the harmonic method.   The values for the airfoil-air mass ratio μ, plunge-to-pitch frequency ratio ω_h/ω_α, and the parameter for the position of the elastic axis a_h, were assumed as 100, 0.1, and -0.5, respectively.

For the cases x_α = 0.3 and 0.4, the flutter speeds at M_∞ = 0.78 are not obtainable from LTRAN2. This difficulty is expected as one observes Fig. 4 for M_c = 0.765. It is seen that the flutter speed increases drastically as the mass center approaches the elastic axis or as x_α becomes smaller. The lower ⋯⋯ of x_ι for obtaining a meaningful flutter speed becomes higher than 0.4 ⋯⋯ ⋯ ⋯ = 0.78.
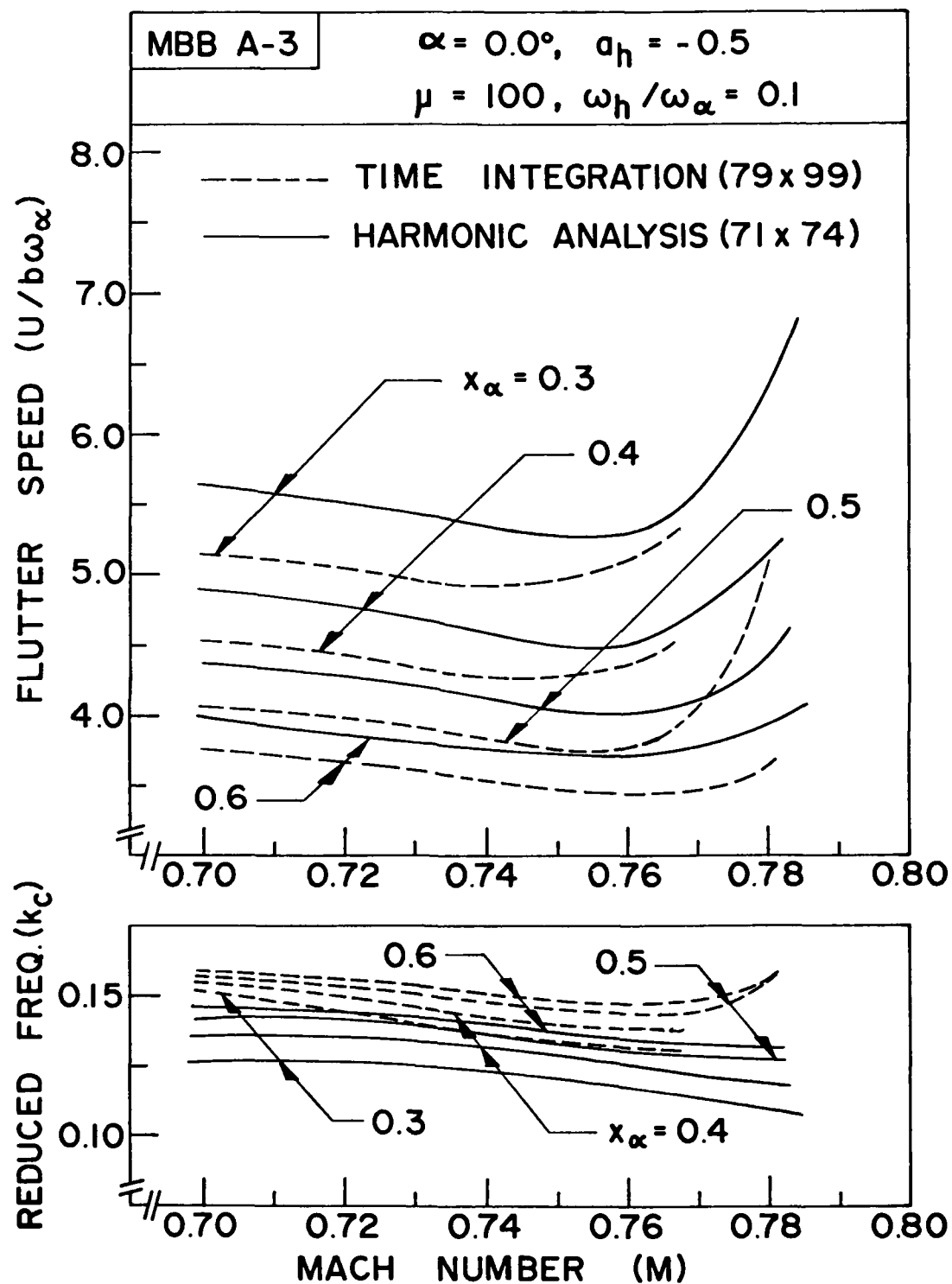
Figure 25.   Effect of Mach Number on Flutter Speed for Four Positions of Mass
Center for MBB A-3 Airfoil at $\alpha = 0.0^{\circ}$.

It is seen in Figure 25 that the flutter speed increases as the mass center approaches the elastic axis or as x_α decreases. All curves for flutter speed present a dip phenomenon. This phenomenon appears to be more pronounced as the mass center moves toward the elastic axis. All the corresponding reduced frequencies are well within the valid range of the two computational methods and programs.

The two sets of curves illustrate similar trends. However, the flutter speeds obtained from the harmonic method are higher than those obtained from the time integration method. The agreement between the two sets of curves is better when the mass center is farther away from the elastic axis. This conclusion has been observed previously in the curves for flutter speed versus x_α (see, for example , Figure 4). The agreement between the two sets of curves becomes worse at higher Mach numbers. This is due to the difference between the two sets of unsteady aerodynamic coefficients given in Tables 6 and 7. The curves obtained from UTRANS2 present a more pronounced dip than the curves obtained from LTRAN2.

Figure 26 shows two sets of curves for flutter speed and the corresponding reduced frequency versus Mach number for three different values of airfoil-air mass ratio (μ = 100, 200, and 300, respectively). The two sets of curves are associated with the two different computational methods. The values for the other aeroelastic parameters x_α, a_h, and ω_h/ω_α were assumed as 0.5, -0.5, and 0.1, respectively.

The two sets of curves agree well. The flutter speeds increase with the increase in airfoil-air mass ratio μ. All curves for flutter speed present a dip phenomenon. The shapes of the dip are fairly similar for all three μ values. All corresponding reduced frequencies are well within the valid range
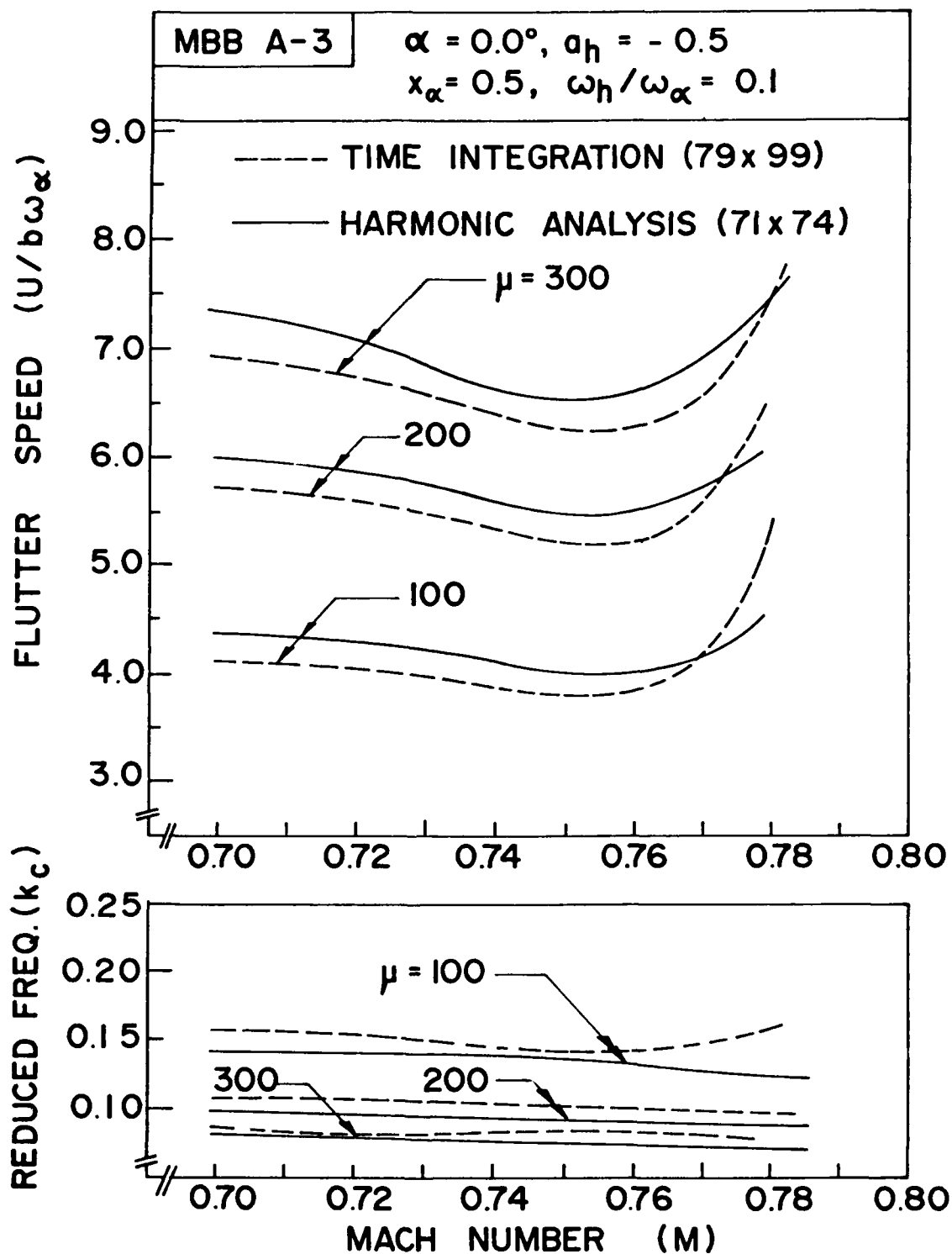
73

Figure 26. Effect of Mach Number on Flutter Speed for Three Airfoil-Air Mass Ratios for MBB A-3 Airfoil at $\alpha = 0.0^{\circ}$.

of the two computer programs.

Figure 27 shows two sets of curves for flutter speed and the corresponding reduced frequency versus Mach number for two different values of plunge-to-pitch frequency ratio (ω_h/ω_α = 0.1 and 0.2, respectively). The two sets are associated with the two different computational methods. The values for the other aero-elastic parameters μ, x_α, and a_h were assumed as 100, 0.5, and -0.5, respectively.

It is seen in Figure 27 that the flutter speed curves for the case ω_h/ω_α = 0.1 are higher than those for the case ω_h/ω_α = 0.2. The two sets of curves, obtained from LTRAN2 and UTRANS2, illustrate similar trends. The flutter speed for ω_h/ω_α = 0.2 and M_α = 0.78 is not obtainable from LTRAN2 data. This is due to the fact that the value of reduced frequency k_c corresponding to the flutter point is beyond the valid range of LTRAN2.

The curves demonstrate the dip phenomenon in the transonic regime. This phenomenon is more obvious in the case ω_h/ω_α = 0.1.

Figure 28 shows two sets of curves for flutter speed and the corresponding reduced frequency versus Mach number for two different positions of elastic axis (a_h = -0.1 and -0.5, respectively). The two sets of curves are associated with the two different computational methods. The aeroelastic parameters x_α, μ, and ω_h/ω_α were assumed as 0.5, 100, and 0.1, respectively.

It is seen in each set of curves that when the position of elastic axis is varied from a_h = -0.1 to a_h = -0.5, there is not much change in flutter speed. The level of agreement between the two sets of curves is similar to that observed in Figures 25 to 27. All the values for the corresponding reduced frequencies are well within the valid range of the two computer programs.

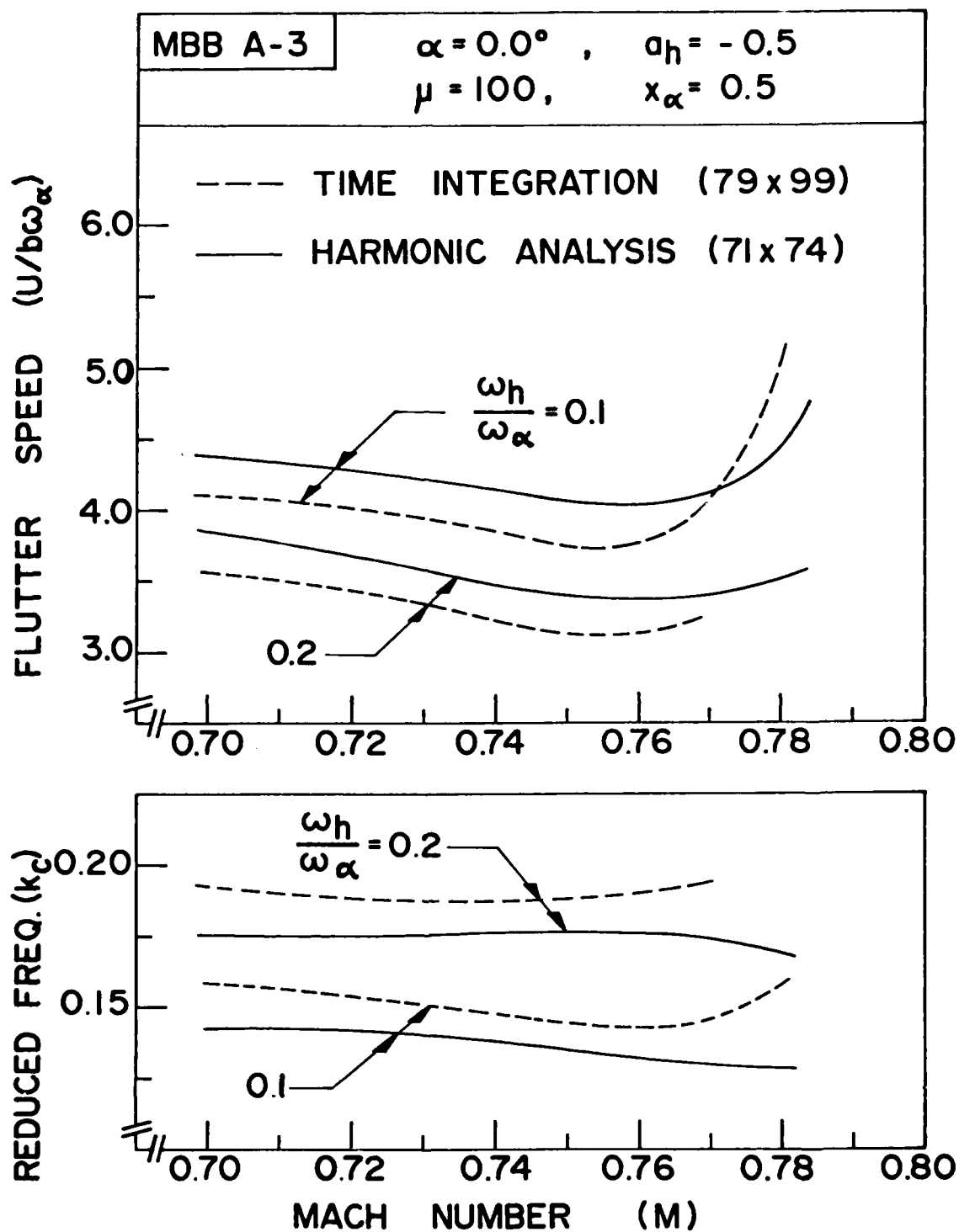All the curves in Figure 28 show that the flutter speed dips in the transonic regime.

75

Figure 27. Effect of Mach Number on Flutter Speed for Two Plunge-to-Pitch Frequency Ratios for MBB A-3 Airfoil at $\alpha = 0.0^0$.
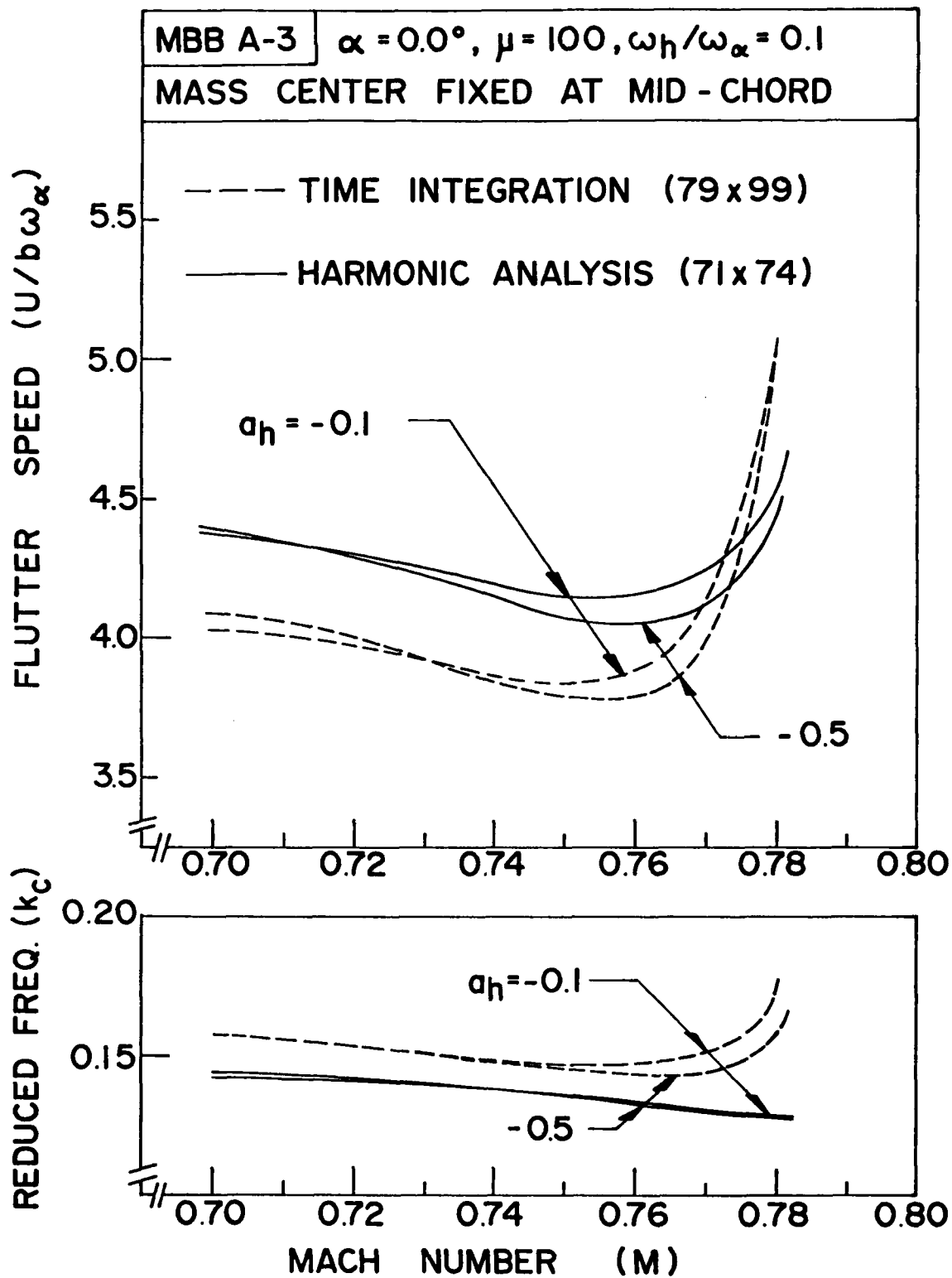
Figure 28. Effect of Mach Number on Flutter Speed for Two Elastic Axis Positions for MBB A-3 Airfoil at $\alpha = 0.0^\circ$.

SECTION VI

CONCLUDING REMARKS

The purpose of this research was to study the flutter behavior of the MBB A-3 supercritical airfoil oscillating with two degrees of freedom in small-disturbance, unsteady transonic flow. Two computer programs, LTRAN2 based on a time integration method, and STRANS2/UTRANS2 based on a harmonic analysis method, were used to compute the aerodynamic coefficients for flutter analysis. For zero mean angle of attack, the results obtained from both methods were directly compared.

For the design conditions of $M_\infty = 0.765$ and an angle of attack that gives a steady lift coefficient of $C_\ell = 0.58$, the aerodynamic and flutter results obtained for the MBB A-3 airfoil were compared to those for a MBB A-3 airfoil without camber, and to those for a NACA 64A010 airfoil scaled down to 8.9% thickness-chord ratio.

The influence of Mach number on flutter speed was studied for the MBB A-3 airfoil at zero mean angle of attack and the transonic dip phenomenon was observed.

As a result of this study, the following concluding remarks may be made:

(1) At the free stream Mach number of 0.765 and zero mean angle of attack, the results for the steady pressure curves, unsteady aerodynamic coefficients, and the flutter speed curves obtained for the MBB A-3 supercritical airfoil based on the two separate computer programs LTRAN2 and STRANS2/UTRANS2 are, in general, in reasonably good agreement.

(2) Within the range of values assumed for all the parameters, it was

found that removal of the camber from the MBB A-3 supercritical
airfoil generally decreases the flutter speed.

(3) The aerodynamic and flutter results obtained for the MBB A-3 airfoil
without camber and those obtained for the conventional NACA 64A010
airfoil scaled down to 8.9% thickness-chord ratio are almost
the same.

(4) For the case of zero mean angle of attack and for the range of
values assumed for the aeroelastic parameters in this study,
it was found that all the curves for flutter speed obtained for
the MBB A-3 supercritical airfoil showed a dip phenomenon
in the transonic regime.

(5) This study shows that the transonic codes LTRAN2 and STRANS2/UTRANS2
can be efficiently used to obtain aerodynamic coefficients for
flutter analysis of an airfoil with supercritical configuration
such as MBB A-3. However, considerably more computing time is
required for the analysis of a supercritical airfoil (e.g. MBB A-3)
than for that of a conventional airfoil (e.g. NACA 64A010).

(6) The discrepancies found between the pressure curves obtained
from the two separate programs may be due to the differences in
mesh size and in the manner the shocks are treated between the
two programs. The differences in steady pressure results contribute
to the disagreement in unsteady coefficients, as the steady results
are used as input for the unsteady computations in both programs.

(7) Due to the low-frequency approximation used in LTRAN2, the reduced
frequencies k_c considered in all of the cases were limited to
be not more than 0.2. Although the low-frequency approximation

was not used in UTRANS2, convergence difficulty was encountered

for higher reduced frequencies. Thus the reduced frequencies

for UTRANS2 were also limited to be not more than 0.2.

(8) As convergence and accuracy both deteriorated with increase in

transonic Mach number and reduced frequency, the highest

reasonable Mach number that could be considered in this study

was 0.78.

(9) For a more complete understanding of the transonic flutter

behavior of supercritical airfoils, the present limitations

on low reduced frequency and low transonic Mach numbers must

be relaxed. Improvements in both computer codes are needed.

(10) Extension of the present 2-D transonic analysis to account

for the 3-D case is needed in order to study more practical

cases of full wing flutter.

(11) Experimental pressure data and flutter trends are needed to

verify the present analytical results.

REFERENCES

1. Whitcomb, R.T. and Clark, L.R., "An Airfoil Shape for Efficient Flight at Supercritical Mach Numbers", NASA TM X-1109 (Confidential report), July 1965.

2. Pearcey, H.H., "The Aerodynamic Design of Section Shapes for Swept Wings", Advances in Aeronautical Sciences, Vol. 3, 1962, pp. 277-322.

3. Montoya, L.C. and Banner, R.D., "F-8 Supercritical Wing Flight Pressure, Boundary Layer, and Wake Measurements and Comparisons with Wind Tunnel Data", NASA TM X-3544, June 1977.

4. Nieuwland, G.Y. and Spee, B.M., "Transonic Shock-Free Flow - Fact or Fiction", AGARD Conference Proceedings 35, Paper 1, 1968.

5. Vincent de Paul, M., "Recherches Experimentales sur des Profiles d'Alles Supercritiques", AGARD Conference Proceedings 35, Paper 13, 1968.

6. Magnus, R., Gallaher, W., and Yoshihara, H., "Inviscid Supercritical Airfoil Theory", AGARD Conference Proceedings 35, Paper 3, 1968.

7. Lock, R.C. and Fulker, J.L., "Design of Supercritical Aerofoils", The Aeronautical Quarterly, Vol. 25, Part 4, November 1974, pp. 245-265.

8. Bauer, F., Garabedian, P., and Korn, D., "Supercritical Wing Sections I", Lecture Notes in Economics and Mathematical Systems, Vol. 66, Springer-Verlag, New York, 1972.

9. Bauer, F., Garabedian, P., Korn, D., and Jameson, A., "Supercritical Wing Sections II", Lecture Notes in Economics and Mathematical Systems, Vol. 108, Springer-Verlag, New York, 1975.

10. Bauer, F., Garabedian, P., and Korn, D., "Supercritical Wing Sections III", Lecture Notes in Economics and Mathematical Systems, Vol. 150, Springer-Verlag, New York, 1977.

11. Sobieczky, H., Yu, N.J., Fung, K-Y., and Seebass, A.R., "New Method for Designing Shock-Free Transonic Configurations", AIAA Journal, Vol. 17, No. 7, July 1979, pp. 722-729.

12. Yang, T.Y., Striz, A.G., and Guruswamy, P., "Flutter Analysis of Two-Dimensional and Two-Degree-of-Freedom Airfoils in Small-Disturbance Unsteady Transonic Flow", AFFDL-TR-78-202, December 1978.

13.   Traci, R.M., Albano, E.D., and Farr, J.L. Jr., "Perturbation
       Method for Transonic Flows About Oscillating Airfoils",
       AIAA Journal, Vol. 14, No. 9, September 1976, pp. 1258-1265.

14.   Ballhaus, W.F. and Goorjian, P.M., "Implicit Finite-Difference
       Computations of Unsteady Transonic Flows About Airfoils,
       Including the Treatment of Irregular Shock-Wave Motions",
       AIAA Paper 77-205, January 1977.

15.   Yang, T.Y., Guruswamy, P., and Striz, A.G., "Aeroelastic
       Response Analysis of Two Dimensional, Single and Two Degree
       of Freedom Airfoils in Low-Frequency, Small-Disturbance
       Unsteady Transonic Flow", AFFDL-TR-79-3077, June 1979.

16.   Ashley, H., "On the Role of Shocks in the 'Sub-Transonic'
       Flutter Phenomenon", AIAA Paper 79-0765, AIAA/ASME/ASCE/AHS
       20th Structures, Structural Dynamics, and Materials Conference,
       St. Louis, Mo., April 4-6, 1979.

17.   Farmer, M.G. and Hanson, P.W., "Comparison of Supercritical
       and Conventional Wing Flutter Characteristics", Proceedings
       AIAA/ASME/SAE 17th Structures, Structural Dynamics, and
       Materials Conference, King of Prussia, Pa., April 1976,
       pp. 608-611.

18.   McGrew, J.A., Giesing, J.P., Pearson, R.M., Zuhuruddin, K.,
       Schmidt, M., and Kalman, T.P., "Supercritical Wing Flutter",
       AFFDL-TR-78-37, March 1978.

19.   Olsen, J.J., "AGARD Standard Configurations for Aeroelastic
       Applications of Transonic Unsteady Aerodynamics, PART III,
       Candidate Airfoil Data", AFFDL-TM-78-6-FBR, January 1978.

20.   Yang, T.Y., Guruswamy, P., Striz, A.G., and Olsen, J.J.,
       "Flutter Analysis of an NACA 64A006 Airfoil in Small Disturbance
       Transonic Flow", To appear in Journal of Aircraft, April 1980.